

UNCLASSIFIED

AD NUMBER

AD801850

LIMITATION CHANGES

TO:

Approved for public release; distribution is unlimited.

FROM:

Distribution authorized to U.S. Gov't. agencies and their contractors; Critical Technology; JUL 1966. Other requests shall be referred to Air Force Materials Laboratory, Metals and Ceramics (MAM), Wright-Patterson AFB, OH 45433. This document contains export-controlled technical data.

AUTHORITY

usafml ltr dtd 29 mar 1972

THIS PAGE IS UNCLASSIFIED

801850

**INVESTIGATION OF NONDESTRUCTIVE METHODS FOR
THE EVALUATION OF GRAPHITE MATERIALS**

Prepared by
AVCO CORPORATION
SPACE SYSTEMS DIVISION
LOWELL, MASSACHUSETTS

TECHNICAL REPORT AFML-TR-66-101

JULY 1966

NOV 14 1966

by
G. E. LOCKYER — E. M. LENOE — A. W. SCHULTZ

This document is subject to special export controls and each transmittal to foreign governments or foreign nationals may be made only with prior approval of the Metals and Ceramics Division (MAM), Air Force Materials Laboratory, Wright-Patterson AFB, Ohio.

**AIR FORCE MATERIALS LABORATORY
RESEARCH AND TECHNOLOGY DIVISION
AIR FORCE SYSTEMS COMMAND
WRIGHT-PATTERSON AIR FORCE BASE, OHIO**

AFML-TR-66-101

**INVESTIGATION OF NONDESTRUCTIVE METHODS FOR
THE EVALUATION OF GRAPHITE MATERIALS**

Prepared by

AVCO CORPORATION

SPACE SYSTEMS DIVISION

LOWELL, MASSACHUSETTS

by

G. E. LOCKYER — E. M. LENOE — A. W. SCHULTZ

This document is subject to special export controls and each transmittal to foreign governments or foreign nationals may be made only with prior approval of the Metals and Ceramics Division (MAM), Air Force Materials Laboratory, Wright-Patterson AFB, Ohio.

FOREWORD

This report was prepared by Avco Corporation, Research and Development Division, Lowell, Massachusetts, under USAF Contract No. AF33(615)-1601. The contract was initiated under Project No. 7360, "The Chemistry and Physics of Materials," Task No. 736002, "Nondestructive Methods." The work was administrated under the direction of the Air Force Materials Laboratory, Research and Technology Division, with Mr. W. L. Shelton, MAMD, acting as project engineer, and Mr. R. R. Rowand, Technical Manager for Nondestructive Methods.

This report covers work conducted from 15 April 1965 to 14 April 1966, at Avco/RAD, Mr. G. E. Lockyer, Project Engineer, and Mr. C. H. Hastings, Project Manager. The work reported on the anisotropic elasticity of graphite, thermal stress wave phenomena, and associated failure mechanisms is the research of Dr. E. M. Lenoë, and the work reported on the infrared technique development and related measurements is the research of Mr. A. W. Schultz. The authors appreciate the contribution of members of the Nondestructive Test Development Group - Messrs. A. M. Chetson, T. M. Ludwig, and E. A. Proudfoot, Group Leader, and members of the Mechanical Test Group - Messrs. A. S. Vaughan, E. Wagner, D. Dowell, and C. L. Theberge.

Manuscript released by the authors May 1966 for publication as an RTD Technical Report.

This technical report has been reviewed and is approved.



W. J. TRAPP
Chief, Strength and Dynamics Branch
Metals and Ceramic Division
Air Force Materials Laboratory

ABSTRACT

A program of investigation was begun in April 1964, to determine nondestructive testing methods and techniques for the evaluation and characterization of graphite materials under contract No. AF33(615)-1601. During the first year, April 1964 to April 1965, the properties and behavior characteristics which are necessary for characterizing graphite as an ablative material for aerospace applications were identified, and applicable NDT methods and techniques were described and theoretically justified. Moreover, the philosophy of Avco's step-wise approach to nondestructive materials evaluation was identified in relation to graphite, and an over-all program plan was established. Correlations between NDT measurements and properties of interest were developed and reported for certain grades of graphite. During the second year, April 1965 to April 1966, these correlations were extended to other grades and, additionally, have been studied in combination in an effort to obtain qualitative response to behavior characteristics such as erosion rate and thermal shock resistance.

To this end, nondestructive test methods for evaluating the performance of graphite under complex thermal and mechanical loading conditions were investigated. The observed response of a molded graphite is compared to theoretical predictions, which are based on the constitutive equations for a transversely isotropic media. Also discussed are the limitations of the theory of anisotropic elasticity as applied to the graphite. Theoretical implications of thermal stress wave phenomena are discussed, and an attempt is made to gain insight into the failure mechanisms of such materials. It is concluded that a temperature dependent Mohr Coulomb yield envelope may be adequate to predict certain aspects of failure in graphite. In addition, realistic thermal shock parameters might be formulated by using detailed experimental investigations of wave phenomena as well as asymptotic solutions to the coupled anisotropic thermoelastic field equations.

In connection with nondestructive thermal properties measurements and related thermal shock studies, a novel technique has been developed to nondestructively determine the near-room-temperature thermal conductivity of graphite. Theory of the technique is presented and is supported by limited experimentation on five good conductors, with emphasis on grain-oriented graphites, to demonstrate its feasibility. The technique involves simultaneously heating the surface of a "semi-infinite" solid with radiant energy and observing the temperature history of this surface using an infrared radiometer as the radiance sensor. Analysis of this history, together with knowledge of the solid's density and heat capacity and comparison with a standard history, yields the conductivity. Results indicate the accuracy of the technique to be within 17 percent of the standard using present equipment.

TABLE OF CONTENTS

	<u>Page</u>
I. Introduction	1
II. Literature and Industrial Survey	3
III. Compilation of Experimental and Theoretical Data	4
IV. Experimental Work and Discussion	7
A. Program Plan	7
B. NDT Screening	7
C. NDT/Mechanical Properties Correlations	7
D. Preliminary Investigation of the Thermo-Mechanical Behavior of Graphite	18
E. Investigation of Infrared Techniques for Nondestructive Determination of Thermal Conductivity	36
V. Conclusions and Recommendations	63
Appendices	66
References	76

LIST OF FIGURES

<u>FIGURE</u>		<u>PAGE</u>
1	Poisson's Ratio (σ) Plotted versus the Function $f(\sigma)$	9
2	Longitudinal Velocity (v_L) versus Dynamic Modulus (E_d) for Grades ATJ, RVA, CFW and CFZ	10
3	Product (ρv_L^2) versus Dynamic Modulus (E_d) for ATJ, RVA, CFW and CFZ	12
4	Product (ρv_L^2) versus Dynamic Modulus (E_d) Extended to Include Grades ZTA and RVA (-1)	13
5	Typical Stress-Strain Plot Showing Relative Positions of (ρv_L^2), Tensile Modulus (E_T) and Secant Modulus (E_S) for a Typical Graphite Tensile Specimen	14
6	Product (ρv_L^2) versus Secant Modulus (E_S) for Grades ATJ, RVA, CFW and CFZ	16
7	Product (ρv_L^2) versus Secant Modulus (E_S) Extended to Include Grades ZTA, RVA (-1) and CFZ	17
8	Typical Molded ATJ Graphite Structure, 210 Magnification, X, Y Plane	19
9	Typical Molded ATJ Graphite Structure, 120 Magnification, X Z Plane	20
10	Illustration of Three Poisson's Ratios in a Molded Graphite	21
11	Torsion Test Fixtures	23
12	Typical Torsion Failures	24
13	Theoretical Uniaxial Modulus Variation	26
14	Theoretical and Observed Shear Modulus Variations	27
15	High Pressure Triaxial Test Apparatus	30
16	Mohr Coulomb Yield Envelope ATJ Graphite With The Grain	31

LIST OF FIGURES (Cont.)

<u>FIGURE</u>		<u>PAGE</u>
17	Mohr Coulomb Yield Envelope ATJ Graphite Against The Grain	32
18	Sketch of Loaded Wedge	34
19	Maximum Pressure as a Function of Wedge Angle for Simple and Mohr Coulomb Yield Criterion	35
20	Theoretical versus Approximate Form Radiation Laws	39
21	Time-Temperature Histories of Materials	47
22	Schematic Diagram of the Experimental Arrangement Used to Measure Thermal Conductivity	51
23	Recordings of Reflected and Self-Emitted Radiation Components from which Emissivities are Determined	54
24	Emissivity and Thermal Conductivity Recordings for a Graphite Specimen	56
25	A Thermal Conductivity Recording of a Large Lead Fabrication, Whose Front Surface Is Coated With Flat Black Lacquer	57
26	Thermal Conductivity of Graphite Specimens Versus Density	61

LIST OF SYMBOLS*

E_1, E_2	-	uniaxial moduli in X_1, X_2 directions
G_{12}	-	shear modulus
ν_2, ν_{21}	-	Poisson's ratios
$\epsilon_1, \epsilon_2, \epsilon_3$	-	uniaxial strains
$\sigma_1, \sigma_2, \sigma_3$	-	uniaxial stresses
$\gamma_{12}, \gamma_{13}, \gamma_{23}$	-	shear strains
τ_{12}, τ_{23}	-	shear stresses
u_1, u_2, u_3	-	displacements
K_1, K_2, K_3	-	thermal conductivities
α_1, α_2	-	coefficients of thermal expansion
C_v	-	specific heat
λ, μ	-	Lame's constants
τ_{max}	-	maximum shear stress in Mohr Coulomb Yield Law
p, p'	-	limiting (plastic) pressure on a wedge

*Symbols pertain to Part D of Section IV. All other symbols are identified in the text.

SECTION I.

INTRODUCTION

Material design parameters and related properties requirements are among the more important considerations in the design of aerospace hardware. Inconsistency in the behavior of graphite materials in ablative applications can be traced to a significant degree to the lack of adequate knowledge of material properties in relation to performance data. The inherent variability within and between billets of various aerospace grades of graphite is evident from the widespread properties data which have been reported. Such evidence suggests that although ineffective design models for ablative applications are a contributing factor, the material variability is the predominant influence affecting graphite's inconsistent behavior. Moreover, because of the wide range in properties that can exist in graphite statistical analysis of random destructive data for a given grade is not sufficient to characterize a given billet or hardware component for ablative environments. As a result, interest has turned to nondestructive testing (NDT) techniques for characterizing graphite for these applications.

The NDT evaluation program which has been conducted on graphite at Avco/RAD was begun in April 1964. The results of the first year's work were published in the final report for that period.⁽¹⁾ The over-all objective of the work has been to develop meaningful nondestructive tests for the evaluation of graphite in thicknesses up to 5 inches. A major part of this activity, which has carried over into the second year, has been concerned with the development of correlations between destructive and nondestructive tests for significant design properties. The success of Avco/RAD's approach in this effort has been described in detail in reference 1. Briefly, this approach depends upon the following:

- 1) Accurate definition of the service significant properties, including a knowledge of the problem areas related to performance and the failure modes and mechanisms which predominate.
- 2) A knowledge of the physical composition of the material, and the variables influencing the properties of interest.
- 3) Selection of the NDT techniques which theoretically should exhibit an interaction with these material variables and, hence, respond to the associated properties.
- 4) Experimental verification of the selected NDT techniques by correlating destructively determined properties with NDT measurements.

This report discusses the work performed on this contract during the second year, April 1965 to April 1966. During this period, correlations between NDT measurements and properties of interest have been extended to include

all the grades identified to be of interest to the Air Force. Additionally, combined use of various NDT techniques and related correlations have been investigated in an effort to obtain qualitative response to behavior characteristics such as erosion rate and thermal shock resistance. Specifically, NDT methods and techniques for evaluating the performance of graphite under complex thermal and mechanical loading conditions were investigated, and a novel technique for nondestructively determining the near-room-temperature thermal conductivity of graphite has been developed. Additional emphasis during the past year has been devoted to the selection of devices which can readily be applied to practical inspection problems concerned with the characterization of graphite for ablative applications.

SECTION II.

LITERATURE AND INDUSTRIAL SURVEY

The literature and consultation survey, which was begun in April 1964, has been carried out as a continuing part of the over-all program. Initially, this survey was aimed at obtaining information concerning destructive and nondestructive testing of graphite, definition and ranking of the service-significant properties and behavior characteristics, and the effects of material processing variables on these service requirements. During the past year, information was also sought as to the performance of graphite components during environmental testing, including failure modes and mechanisms in an effort to determine the extent to which such failures could be identified with materials variability. To date, however, only limited information has been revealed which attempts to link graphite material properties variations to environmental performance, and this information is mostly concerned with erosion rate for subscale rocket nozzle inserts as related to porosity.

SECTION III

COMPILATION OF EXPERIMENTAL AND THEORETICAL DATA

The experimental and theoretical compilation has also continued throughout the second year. A detailed discussion of this work for the first year, including tables relating property and behavior characteristics to influencing materials variables, and the interaction of the selected NDT energy with these variables, was also presented in Reference 1. Also included in that discussion was a theoretical justification for applying each selected NDT technique, namely, ultrasonic velocity and its relation to modulus and density, radiography for flaw detection, and radiometry for measurement of local bulk density. Theory and justification for use of transient infrared techniques for determining thermal properties were also presented briefly, and will be covered in detail in a later section of this report. Each of these NDT techniques is applicable to practical inspection and evaluation of graphite billets and hardware components.

From the more significant design properties for ablative applications, modulus of elasticity, tensile strength and strain-to-failure, thermal conductivity and thermal expansion were selected for study. Developing the NDT capability for determining each of these properties at room temperature, or near-room temperature, is justification for the correlation studies which have been performed on each property. However, in addition to this single importance of each of these properties is their combined significance in relation to behavior characteristics such as erosion rate and thermal shock resistance.

The importance of erosion rate and thermal shock resistance in graphite rocket nozzle applications, has been noted by other investigators. ^(2, 3) These workers report on the effects of porosity on erosion rate for subscale nozzle inserts during solid propellant rocket motor firings. C. E. Waylett et al (Reference 2), for example, show significant data for an erosion rate parameter versus bulk density for nozzle inserts of several grades of graphite. This is particularly significant from the viewpoint of NDT since local variations in bulk density of discrete volumes in billets and nozzles can be determined nondestructively by radiometric gauging. Berard and Swope (Reference 3) describe the effects of size and distribution of open porosity on erosion rate for some fifteen grades of graphite. Moreover, they give a detailed description, as do other sources in the literature, ⁽⁴⁾ of how to measure the size of open porosity by mercury intrusion techniques. Again, from the viewpoint of NDT, measurement of open porosity coupled with local measurements of bulk density, from which distribution of total volume porosity can be assessed, is significant.

The occurrence of failures caused by thermal shock and related properties variability are not reported by either of the investigating teams referenced above, although the ability to withstand thermal shock is recognized by Waylett, et al, as being a prime factor for determining the suitability of graphite for nozzle applications. It should be mentioned that, since neither of the programs referenced

above was designed to evaluate thermal shock resistance, it may be that the environmental conditions used were not sufficient in degree and/or duration to induce this kind of failure.

In any case, data on ablative performance of graphite materials versus thermal shock and related properties has not been noted in the literature to date. However, references to a qualitative parameter for describing the resistance of high-temperature refractory materials to fracture by thermal shock have been noted in the literature (5,6). This parameter has been expressed as:

$$F = \frac{k S}{\alpha E} \quad (1)$$

where: k = thermal conductivity
S = tensile strength
 α = coefficient of thermal expansion
E = modulus of elasticity

Nondestructive determinations of tensile strength and modulus have been presented previously, and will be discussed in some detail in Section IV of this report. The coefficient of thermal expansion and thermal conductivity, however, are not easily handled insofar as nondestructive measurement is concerned, although the possibility of obtaining a nondestructive assessment of thermal expansion is suggested from the following relationship between thermal expansion and other properties in crystalline isotropic metals:

$$\frac{K \alpha}{\rho C_v} = Q(\text{a constant}) \quad (2)$$

where: K = bulk modulus
 α = coefficient of thermal expansion
 ρ = density
 C_v = heat capacity at constant volume

Substituting for α from equation (2) into equation (1), we obtain:

$$F = \frac{k K S}{\rho C_v E Q} \quad (3)$$

D. Preliminary Investigation of the Thermo-Mechanical Behavior of Graphite

Several investigators^(7, 8) have suggested that, because of the complex combinations of failure mechanisms that may occur, prediction of the behavior of potential rocket nozzle materials based on physical property data or simple laboratory tests is difficult, if not impossible.

For graphite, this is in part due to ignorance of the true failure mechanisms of such materials and also partly attributable to a general over-confidence in simple mathematical idealization of graphitic mechanical and thermal behavior. In this discussion, the widely applied assumption of plane isotropy is first presented, and an effort is then made to delineate some of the controlling influences of actual response phenomena.

Typical microstructure of molded ATJ graphite is illustrated by the photomicrographs, Figures 8 and 9. The non-uniform density as well as the inherent porosity is clearly revealed by these magnified views of the material. Due to observed anisotropy and the nature of the molding process, a widely suggested form of constitutive equations is that associated with plane isotropy.

Evaluations of the material are usually performed in two directions normally identified as "with the grain" and "against" or "across the grain." It has been stated that seven interrelated elastic constants (five independent constants) describe the stress-strain behavior of the graphite^(9, 10), namely, three different Poisson's ratio (see Figure 10), two uniaxial moduli, and two shear moduli.

At this point, it is well to emphasize that this mathematical model for stress-strain response has the inherent limitations of:

- a. linear stress-strain behavior
- b. no distinction between tensile and compressive properties.

In reality (see Reference 9, page 7), for both grain orientations, the tensile and compressive properties differ; the compressive moduli being lower than the tensile moduli in room temperature tests and higher in elevated temperature tests. As far as lateral strain for uniaxial loading is concerned, two of the three Poisson's ratios are about the same over a wide temperature range and the third is considerably higher.

The transformation equations, which predict elastic constant variations as a function of orientation to the directions of anisotropy, are readily available and stated in the form:

$$\frac{1}{E(\phi)} = \frac{\sin^4 \phi}{E_2} + \left(\frac{1}{G_{12}} - \frac{2\nu_{12}}{E_1} \right) \sin^2 \phi \cos^2 \phi + \frac{\cos^4 \phi}{E_1} \quad (10)$$

SECTION IV.

EXPERIMENTAL WORK AND DISCUSSION

A. Program Plan

During the past year the program plan was one of essentially two phases. The first phase involved the extension of the NDT/mechanical properties correlations, which began during the first year, to all graphite grades of interest to the Air Force. Grades worked on were Union Carbide's ATJ, RVA, CFW, CFZ, ZTA, and a special grade designated as RVA (-1); the RVA (-1) billet was so designated because it was processed to within one step of completely processed RVA. The second phase of the program was concerned with developing correlations between NDT and other properties and behavior characteristics for these same grades. As in the past, the program plan called for a three-stage evaluation approach; the graphite billet, selected sections and specimen blanks, and the final destructive test specimen. Of course, actual correlation of destructively determined properties with NDT response provided the experimental verification of the applicability of the various NDT techniques. Practical NDT measurement and/or inspection systems for implementing these correlations on graphite billets and hardware were also a primary consideration.

B. NDT Screening

Screening of billets for sectioning and selection of specimen blanks to embrace the maximum range of material variability was performed by ultrasonic velocity and radiometry measurements. Both of these NDT measurements are sensitive to variations in density, which has been identified and experimentally verified to be the predominant material variable affecting the properties of interest. Radiometry can be used to obtain a direct measurement of density to within $\pm 1\%$. Velocity measurements, in addition to their sensitivity to density, are sensitive to the material anisotropy and to elastic properties. A combination of radiometrically determined density and longitudinal wave velocity is uniquely correlatable to other properties of interest, as will be discussed later. These reasons provide sufficient justification for the use of these readily applied state-of-the-art techniques for the required screening. Moreover, at the present state of development, other NDT techniques, such as infrared and eddy current, do not supply significant screening capabilities beyond those stated above. For a more detailed description of screening techniques, as well as examples of typical variations within and between billets, the reader is referred to last year's final report (Reference 1).

C. NDT/Mechanical Properties Correlations

The relationship of the longitudinal-wave velocity to dynamic modulus and density has been discussed in detail in previous reports, and may be expressed as:

$$v_L^2 = \frac{E_D (1 - \sigma)}{\rho (1 + \sigma) (1 - 2\sigma)} \quad (5)$$

where (E_D), (ρ) and (σ) are the dynamic modulus, density and Poisson's ratio, respectively.

An attempt was made to determine the effect of Poisson's ratio in this expression. To do this it was first necessary to obtain the range of values to be expected for σ in representative grades. Poisson's ratio was calculated on 18 selected specimens of ATJ and 10 selected specimens of RVA from measurements of transverse-wave velocity (V_T) and longitudinal-wave velocity (V_L) using the relationship:

$$\sigma = \frac{1 - 2(V_T/V_L)^2}{2 - 2(V_T/V_L)^2} \quad (6)$$

It should be noted that the specimens selected were designed to cover the widest range of material variability available in these grades, both with and against the grain. Although the above expression is only strictly valid for an isotropic material, the calculations obtained were felt to be sufficiently accurate to identify the range of (σ) to be expected, which in all cases was calculated to be less than 0.20. As added support, 6 determinations of (σ) were made on CFW graphite by compression testing (4 against the grain and 2 with the grain). The maximum value obtained against the grain was 0.15, while the maximum obtained with the grain was 0.11, which is within the range identified from the calculations above.

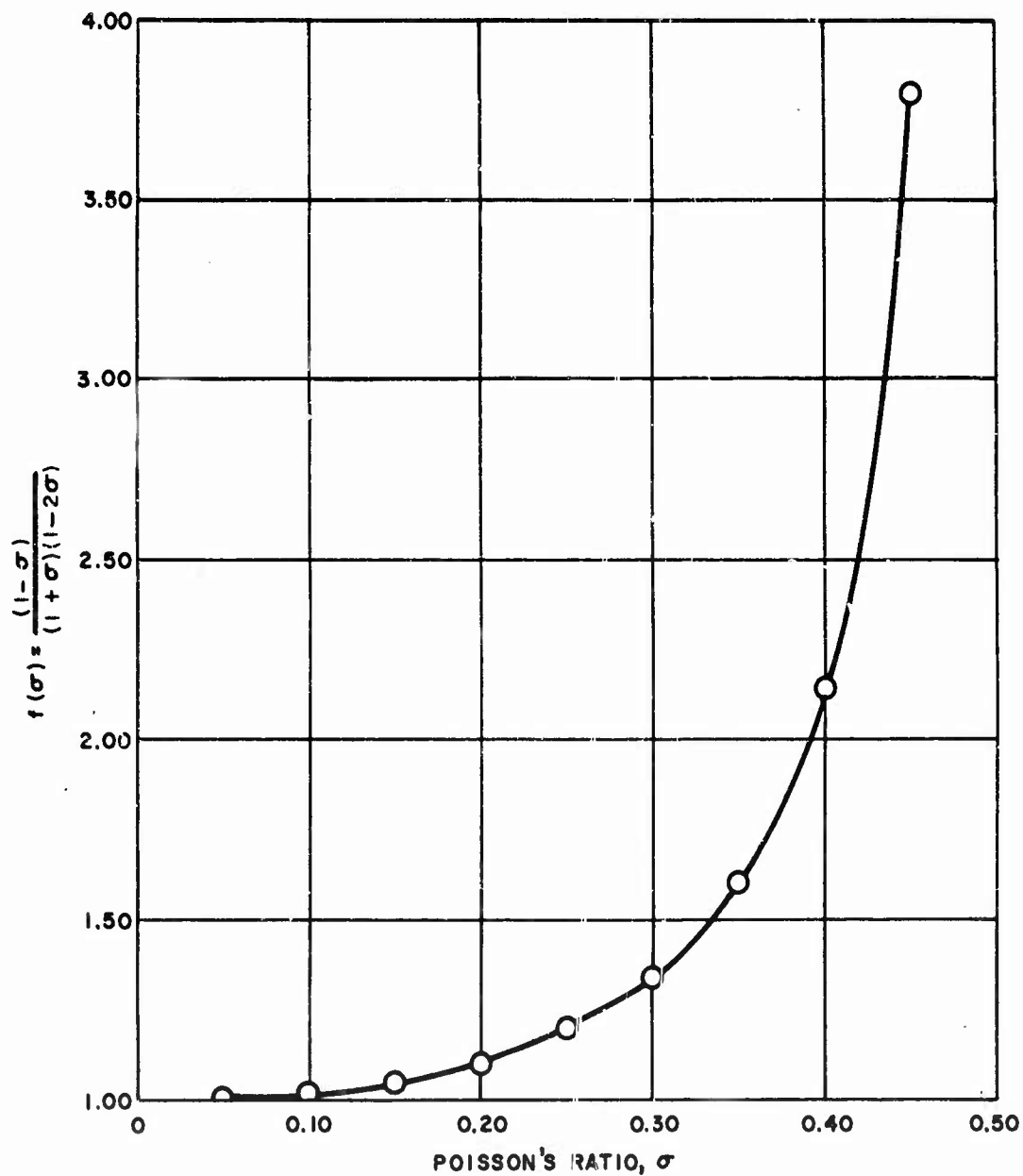
The function $f(\sigma) = \frac{(1 - \sigma)}{(1 + \sigma)(1 - 2\sigma)}$ in equation (5) has been graphed versus (σ) in Figure 1. Note that for positive values of (σ), the function $f(\sigma)$ has the limiting value of 1.00 for $\sigma =$ zero, and becomes infinite at $\sigma = 0.50$. Also, for values of (σ) less than 0.20, $f(\sigma)$ is less than 1.10. For our purposes then, equation 5 may be written as:

$$V_L^2 = \frac{E_D}{\rho} \quad (7)$$

This expression may in turn be written as:

$$\log V_L = 1/2 \log E_D - 1/2 \log \rho \quad (8)$$

For purposes of analyzing the data, it is sometimes more convenient to work with equation 8 since log-log displays of the data involve straight line relationships. Figure 2 is a graph of such a plot for Union Carbide grades ATJ, RVA, CFW, and CFZ. The data from any given billet, with and/or against the grain, fits a given line; the ATJ data for both directions, by virtue of its lower density, on the upper line and the other grades of higher density on the lower line. The sensitivity to approximately a 5 percent difference in average density between ATJ and the other grades is noted to be a significant vertical displacement in the graphs. Furthermore, the slopes of the lines are approximately 1/2 as predicted by equation (8).



760333D

Figure 1 POISSON'S RATIO (σ) PLOTTED VERSUS THE FUNCTION

$$f(\sigma) = \frac{(1-\sigma)}{(1+\sigma)(1-2\sigma)}$$

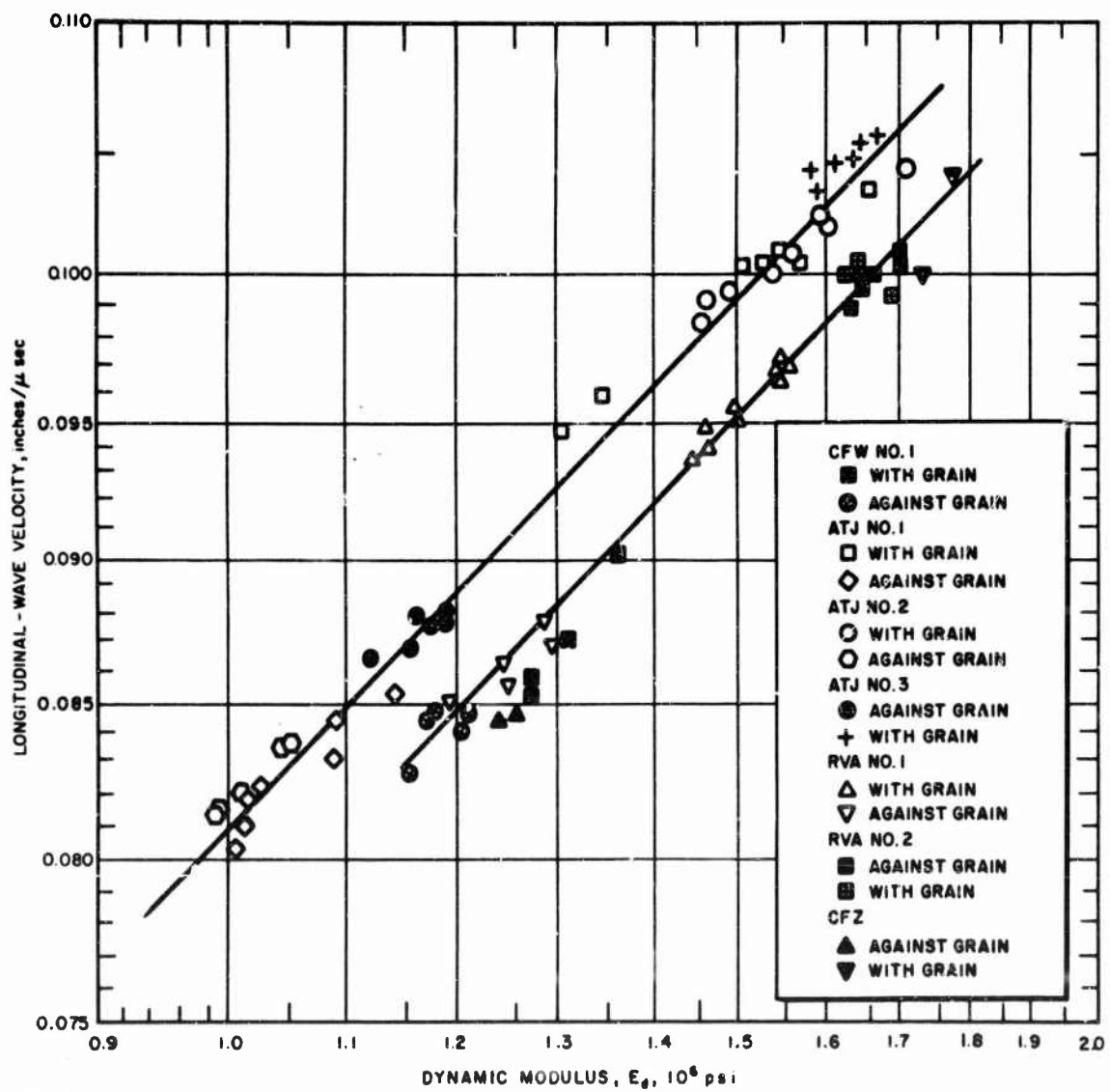


Figure 2 LONGITUDINAL VELOCITY (V_L) VERSUS DYNAMIC MODULUS (E_d)
FOR GRADES ATJ, RVA, CFW, AND CFZ

Another useful way of presenting this data is that shown in Figure 3. Here, (ρV_L^2) is plotted as a function of the dynamic modulus (E_D) and is a more useful graph since nondestructively measurable quantities (ρ and V_L) are plotted versus a property of interest. Figures 2 and 3 provide the experimental verification of the relationship shown in equations (7) and (8). The log-log display was presented to illustrate the effect of density since it has been identified as the first-order material variable which influences properties and behavior characteristics of interest. Practical aspects are that the independent nondestructive measurement of velocity and density can be used to determine dynamic elastic modulus, both with and against the grain to within approximately $\pm 0.06 \times 10^6$ psi in billets and hardware components of these grades of graphite.

The data from grades ZTA and RVA (-1) were deliberately omitted from the graphs of Figures 3 and 4 because the range of values far exceeded those of the other grades plotted. For the 16 ZTA specimens shipped to Avco for evaluation (5 specimens with the grain and 10 against) values of dynamic modulus ranged from 0.77×10^6 psi against the grain to 3.39×10^6 psi for specimens with the grain. Specimens of RVA (-1) (2 with the grain and 2 against the grain), ranged from 1.83×10^6 psi to 2.71×10^6 psi. To illustrate the range of these values compared to the other grades tested and plotted in Figure 3, consider the graph of Figure 4. The solid line is the graph of the data for the grades shown in Figure 3, while the dotted line represents the extension of the graph, with and against the grain, to include the ZTA data. It is significant to note that, within the same scatter as shown for the data in Figure 3, the ZTA data fits the same line. The change in intercept for the RVA (-1) data has not been explained. However, it has been noted that dynamic modulus measurements by the resonance beam technique were difficult to obtain on this material because of poor definition of the resonant frequency.

Having completed all the required nondestructive testing on the specimen blanks for the various billets of each grade, selected specimen blanks covering the desired range of NDT variability were machined into tensile bars for destructive mechanical evaluation. Longitudinal-wave velocity was measured along the axis of each tensile specimen to obtain data in the direction of loading prior to tensile testing. Radiographs of each tensile specimen were also taken to assess macroscopic flaw content and thereby avoid extraneous data which might be caused by flaws.

Establishing an NDT/tensile strength correlation involved some rather unique considerations. To illustrate these ideas, consider Figure 5, which shows a stress-strain curve for a typical specimen from a given direction in a typical billet of graphite. Also shown in the figure is the graph of a line whose slope is numerically equal to the product (ρV_L^2) for that specimen. The value of density in this case was taken from a section of the tensile specimen adjacent to the fracture and, as noted earlier, (V_L) was measured along the axis of the specimen prior to loading. It will be remembered that for our purposes (ρV_L^2) was noted to be equal to the dynamic modulus (E_D). Figure 5 also shows the secant modulus

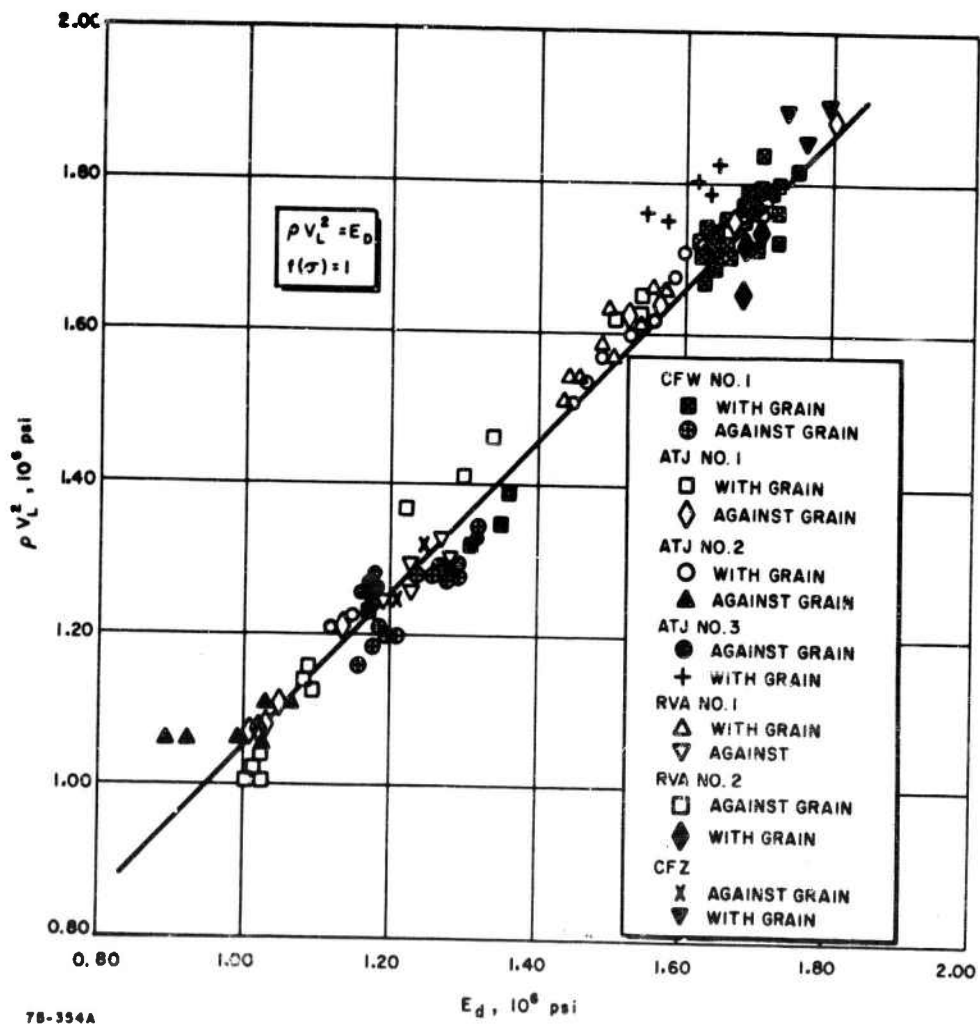
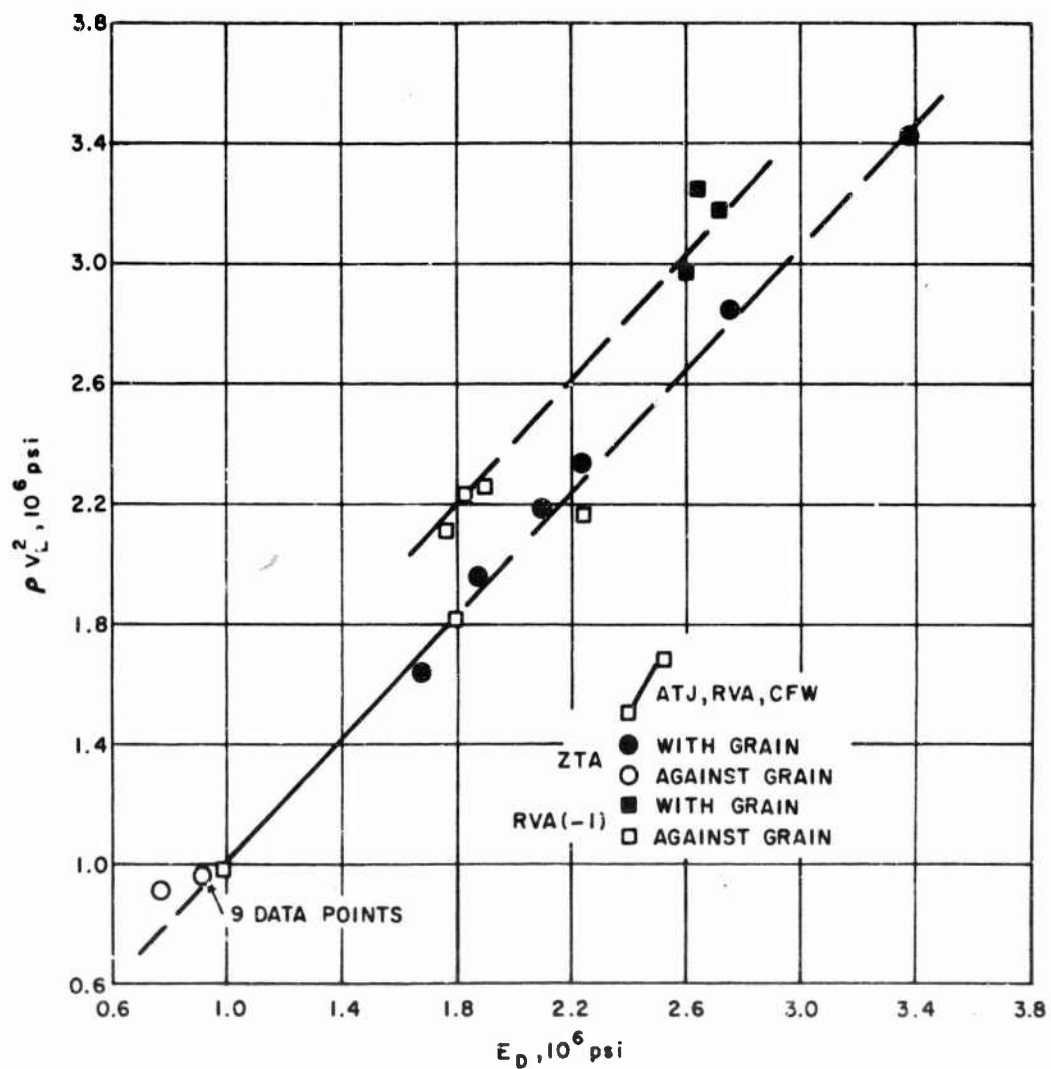
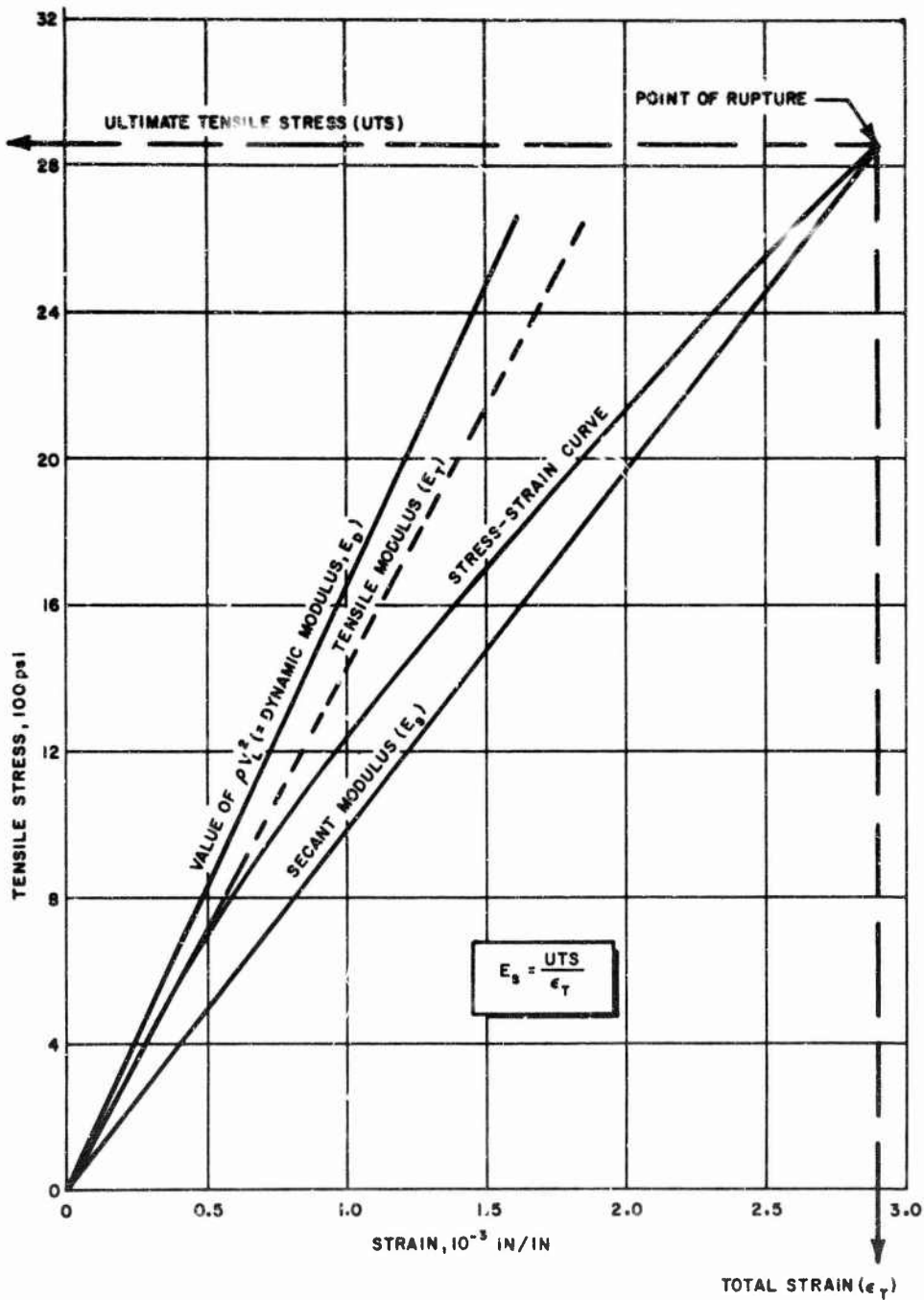


Figure 3 PRODUCT (ρV_L^2) VERSUS DYNAMIC MODULUS (E_d) FOR ATJ, RVA, CFW AND CFZ



760334D

Figure 4 PRODUCT (ρV_L^2) VERSUS DYNAMIC MODULUS (E_D) EXTENDED TO INCLUDE GRADES ZTA AND RVA (-1)



75-436

Figure 5 TYPICAL STRESS-STRAIN PLOT SHOWING RELATIVE POSITIONS OF (ρV_L^2) , TENSILE MODULUS (E_T) AND SECANT MODULUS (E_S) FOR A TYPICAL GRAPHITE TENSILE SPECIMEN

taken from origin to failure on the stress-strain curves. The secant modulus is defined here as:

$$E_s = \frac{\text{Ultimate Tensile Stress (UTS)}}{\text{Total Strain to Failure } (\epsilon_T)}$$

Analysis of the tensile data revealed that the ratio of (ρv_L^2) to (E_s) was essentially a constant for a given direction in a given grade of graphite. Figure 6 is a plot of (ρv_L^2) versus the secant modulus (E_s) for specimens taken with and against the grain from grades ATJ, RVA, CFW and CFZ. Actual ultimate tensile stress and total strain-to-failure on each individual specimen were used to calculate (E_s) . Since graphite is brittle at room temperature, variations in total strain between specimens of the same direction in a given grade are noted to be small. Therefore, for purposes of determining ultimate tensile strength from the graph, the total strain for specimens from the same direction of the same grade is taken to be constant; the average values being used in each case.

In practice, the density (ρ) and the velocity (v_L) are nondestructively measurable quantities which can be obtained on billets and hardware. A given value of (ρv_L^2) corresponds, within the limits shown, to the secant modulus. By multiplying the secant modulus by the average total strain for a given direction of a given grade of graphite, the ultimate tensile strength may be determined to within approximately ± 300 psi. This range is well within the range of values normally reported for this property in these grades at room temperature.

Again, the data from grades ZTA and RVA (-1) was deliberately omitted from the graph of Figure 6 because, as noted for the ρv_L^2 /dynamic modulus correlation of Figure 4, the range of values far exceeded that of the other grades. Secant modulus ranged from as low as about 0.70×10^6 psi against the grain to about 3.4×10^6 psi with the grain, which is approximately 3 times the range noted for the other grades tested. Specimens of RVA (-1) ranged from 1.25×10^6 psi against the grain to 1.98×10^6 psi with the grain. Figure 7 shows the values of data for the grades plotted in Figure 6, while the dotted line represents the extension of the correlation, with and against the grain, to include the ZTA and RVA (-1) data. It is significant to note that, as was the similar case for the dynamic modulus correlation, the ZTA and RVA (-1) data fits the same line, which supports the validity of the analysis which led to these correlations.

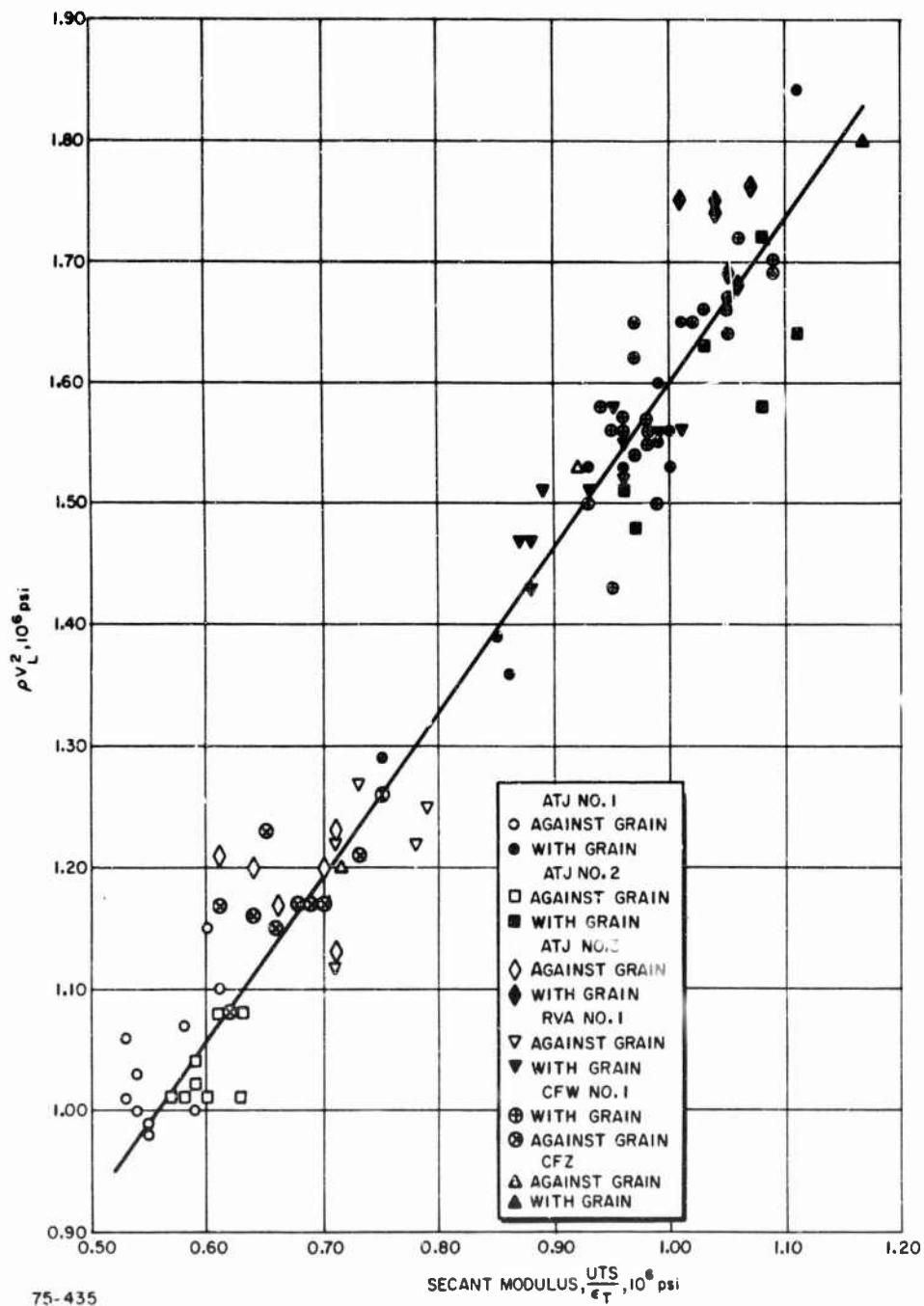
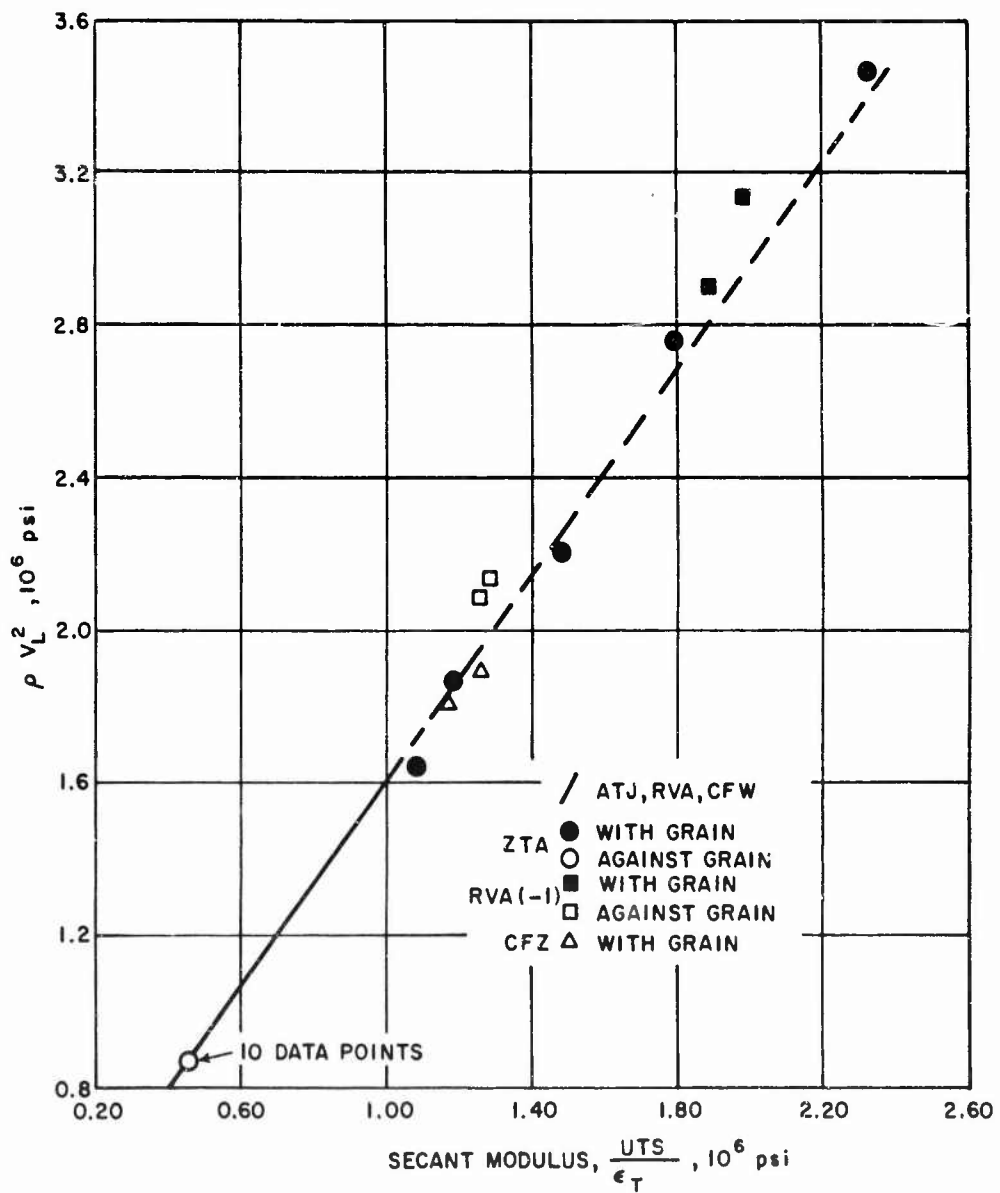


Figure 6 PRODUCT (ρV_L^2) VERSUS SECANT MODULUS (E_s) FOR GRADES ATJ, RVA, CFW AND CFZ



780335D

Figure 7 PRODUCT (ρV_L^2) VERSUS SECANT MODULUS (E_s) EXTENDED TO INCLUDE GRADES ZTA, RVA (-1) AND CFZ

D. Preliminary Investigation of the Thermo-Mechanical Behavior of Graphite

Several investigators^(7, 8) have suggested that, because of the complex combinations of failure mechanisms that may occur, prediction of the behavior of potential rocket nozzle materials based on physical property data or simple laboratory tests is difficult, if not impossible.

For graphite, this is in part due to ignorance of the true failure mechanisms of such materials and also partly attributable to a general over-confidence in simple mathematical idealization of graphitic mechanical and thermal behavior. In this discussion, the widely applied assumption of plane isotropy is first presented, and an effort is then made to delineate some of the controlling influences of actual response phenomena.

Typical microstructure of molded ATJ graphite is illustrated by the photomicrographs, Figures 8 and 9. The non-uniform density as well as the inherent porosity is clearly revealed by these magnified views of the material. Due to observed anisotropy and the nature of the molding process, a widely suggested form of constitutive equations is that associated with plane isotropy.

Evaluations of the material are usually performed in two directions normally identified as "with the grain" and "against" or "across the grain." It has been stated that seven interrelated elastic constants (five independent constants) describe the stress-strain behavior of the graphite^(9, 10), namely, three different Poisson's ratio (see Figure 10), two uniaxial moduli, and two shear moduli.

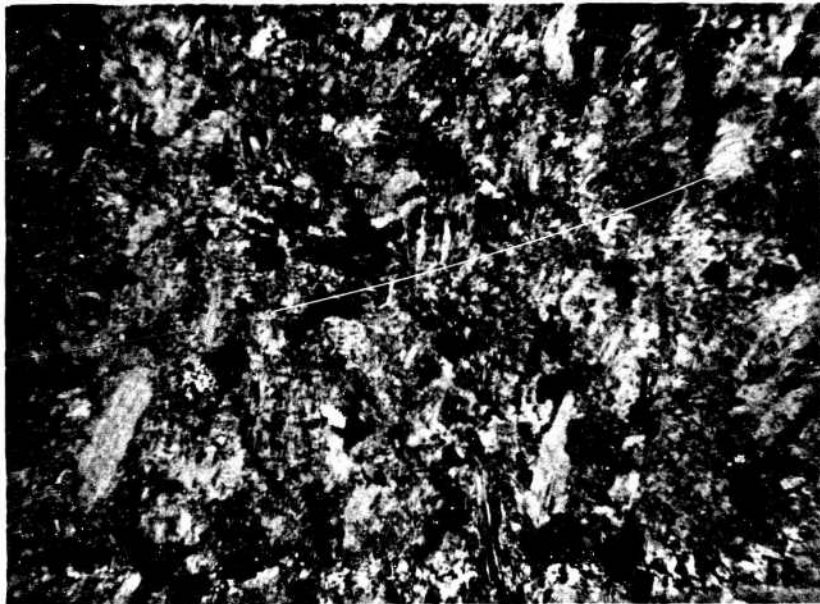
At this point, it is well to emphasize that this mathematical model for stress-strain response has the inherent limitations of:

- a. linear stress-strain behavior
- b. no distinction between tensile and compressive properties.

In reality (see Reference 9, page 7), for both grain orientations, the tensile and compressive properties differ; the compressive moduli being lower than the tensile moduli in room temperature tests and higher in elevated temperature tests. As far as lateral strain for uniaxial loading is concerned, two of the three Poisson's ratios are about the same over a wide temperature range and the third is considerably higher.

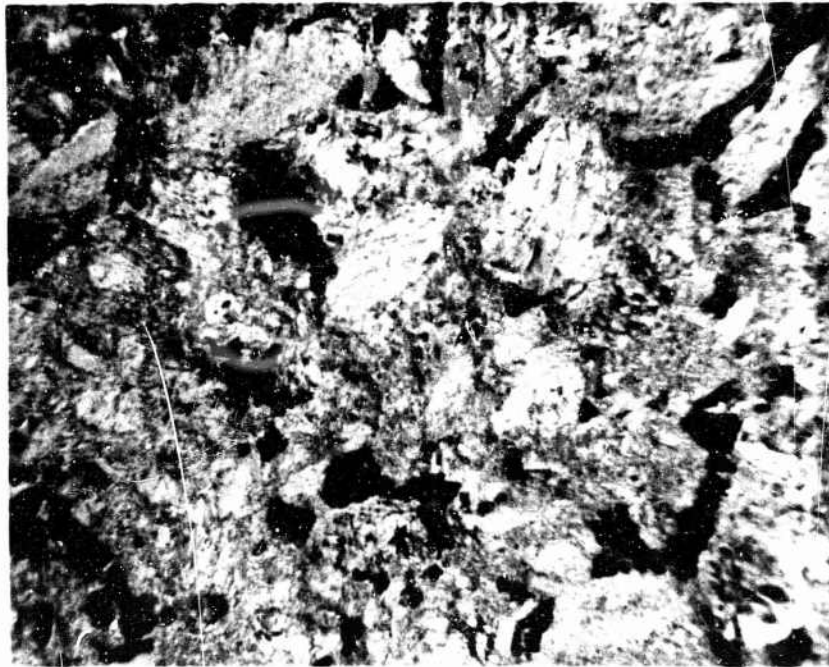
The transformation equations, which predict elastic constant variations as a function of orientation to the directions of anisotropy, are readily available and stated in the form:

$$\frac{1}{E(\phi)} = \frac{\sin^4 \phi}{E_2} + \left(\frac{1}{G_{12}} - \frac{2\nu_{12}}{E_1} \right) \sin^2 \phi \cos^2 \phi + \frac{\cos^4 \phi}{E_1} \quad (10)$$



76036D

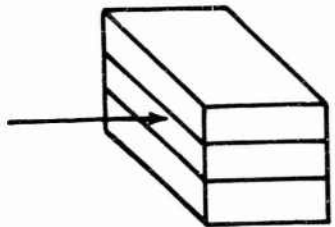
Figure 8 TYPICAL MOLDED ATJ GRAPHITE STRUCTURE, 210X, X, Y PLANE



700337D

Figure 9 TYPICAL MOLDED ATJ GRAPHITE STRUCTURE, 120X, X Z PLANE

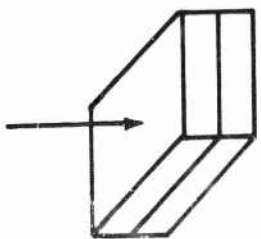
LOAD WITH GRAIN



$$\text{POISSON'S RATIO} = \frac{\epsilon' \text{ LATERAL WITH GRAIN}}{\epsilon' \text{ AXIAL WITH GRAIN}}$$

$$\text{POISSON'S RATIO} = \frac{\epsilon' \text{ LATERAL ACROSS GRAIN}}{\epsilon' \text{ AXIAL WITH GRAIN}}$$

LOAD ACROSS GRAIN



$$\text{POISSON'S RATIO} = \frac{\epsilon' \text{ LATERAL WITH GRAIN}}{\epsilon' \text{ AXIAL ACROSS GRAIN}}$$

760380

Figure 10 ILLUSTRATION OF THREE POISSON'S RATIO IN A MOLDED GRAPHITE

where: $E(\phi)$ is the uniaxial modulus at angle ϕ to the X_1 direction,
 E_1, E_2 are the uniaxial moduli in X_1, X_2 directions
 G_{12} is the appropriate shear modulus
 ν_{12} is the Poisson's ratio

$$\frac{1}{G_{12}(\phi)} = 4 \left(\frac{1}{E_1} + \frac{1}{E_2} + \frac{2\nu_{12}}{E_1} - \frac{1}{G_{12}} \right) \sin^2 \phi \cos^2 \phi + \frac{1}{G_{12}}$$

However, a relatively thorough literature survey did not yield any information as to the validity of such a predicted properties variation. Preliminary studies were completed in this area. Eight torsion samples were machined from a typical ATJ billet, and velocity measurements made as listed in Table I, with the associated dynamic moduli determined from correlation data reported in Section IV-C.

TABLE I

Uniaxial Modulus Properties of the Torsion Samples

<u>Sample Number</u>	<u>Direction</u>	<u>Velocity in/μ sec.</u>	<u>Approximate Dynamic Modulus, psi</u>
1	Y	.1047	1.68×10^6
2	Y	.1058	
3	X	.0888	1.19×10^6
4	X	.0886	
5	Z	.1009	1.52×10^6
6	X	.1017	
7	45° in YZ	.1020	1.58×10^6
8	plane	.1020	

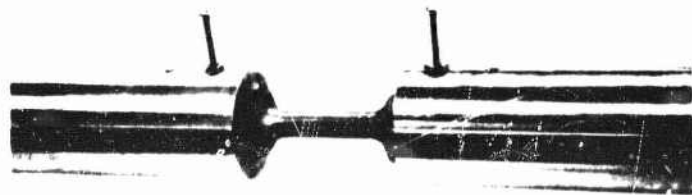
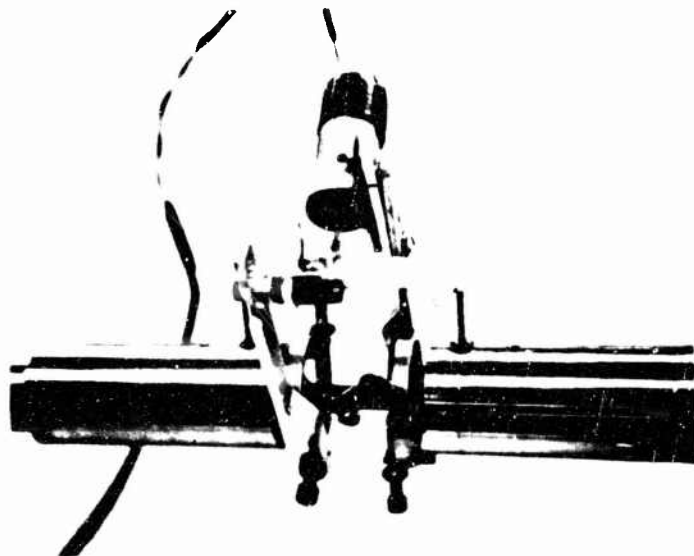
Inspection of the dynamic modulus values suggests that the YZ plane departs from assumed isotropy.

The torsion test data is listed in Table II. Sample geometry and test fixtures are shown in Figure 11 and typical torsion failures illustrated by Figure 12.

TABLE II

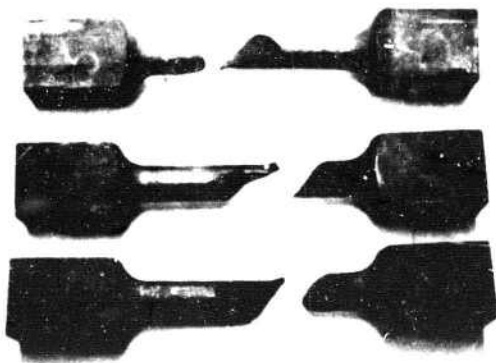
Torsion Test Results

<u>Sample No.</u>	<u>Axis</u>	<u>Shear Modulus</u>	<u>Shear Strength</u>
1	Y	$.641 \times 10^6$ psi	3830 psi
2	Y	$.678 \times 10^6$	3960
3	X	$.569 \times 10^6$	3560
4	X	$.561 \times 10^6$	3750



760389D

Figure 11 TORSION TEST FIXTURES



760340D

Figure 12 TYPICAL TORSION FAILURES

TABLE II (Cont'd)

<u>Sample No.</u>	<u>Axis</u>	<u>Shear Modulus</u>	<u>Shear Strength</u>
5	Z	$.625 \times 10^6$ psi	3460 psi
6	Z	$.613 \times 10^6$	3880
7	45° in YZ	$.643 \times 10^6$	4070
8	45° in YZ	$.595 \times 10^6$	3400

It has been suggested⁽⁹⁾ that torsion tests are not appropriate for shear properties determinations since tensile stresses induce the actual fracture. From this point of view, it is interesting to note that the maximum shear strengths reported in Table II are in rather close agreement with data presented in Reference 9. In the same reference, a notched bar shear test is advocated for both shear moduli and shear strength observations. However, data reported in that study indicates gage length effects on both modulus and shear strength.

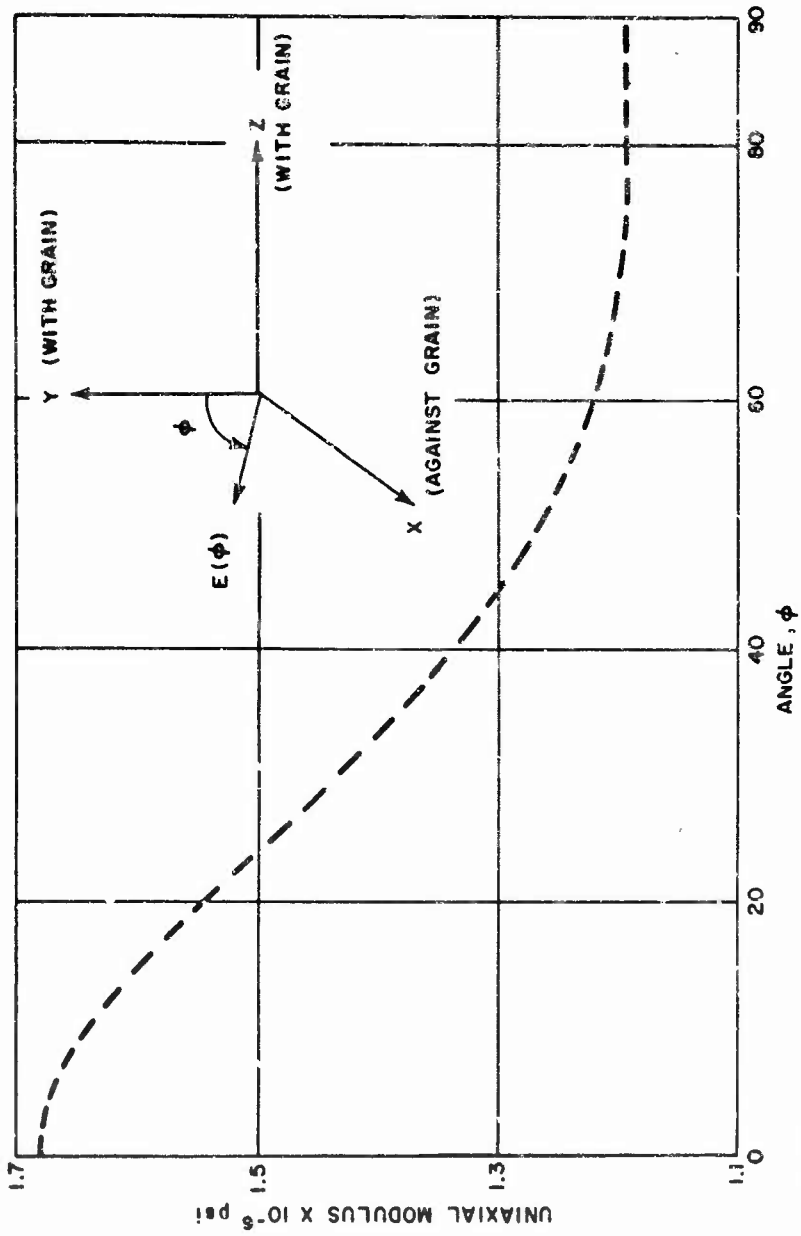
Therefore, it is currently believed that the shear moduli determined from torsion tests are reliable. In order to substantiate the shear modulus measurement, two torsional resonance vibration tests were performed on circular bars and the resulting shear modulus values were in excellent agreement with the torsion test data.

Figure 13 illustrates theoretical uniaxial modulus variation and Figure 14 presents a comparison of predicted and observed shear modulus. Fair agreement seems evident. Keeping in mind the known thermal effects on mechanical properties of the graphite, it is suggested that a valuable experimental program would involve a comparison of mechanical response at various orientations over a wide temperature range.

It has been demonstrated by means of wave velocity measurements that departures from isotropy exist in the YZ plane, that the shear modulus variation approximates theoretical predictions.

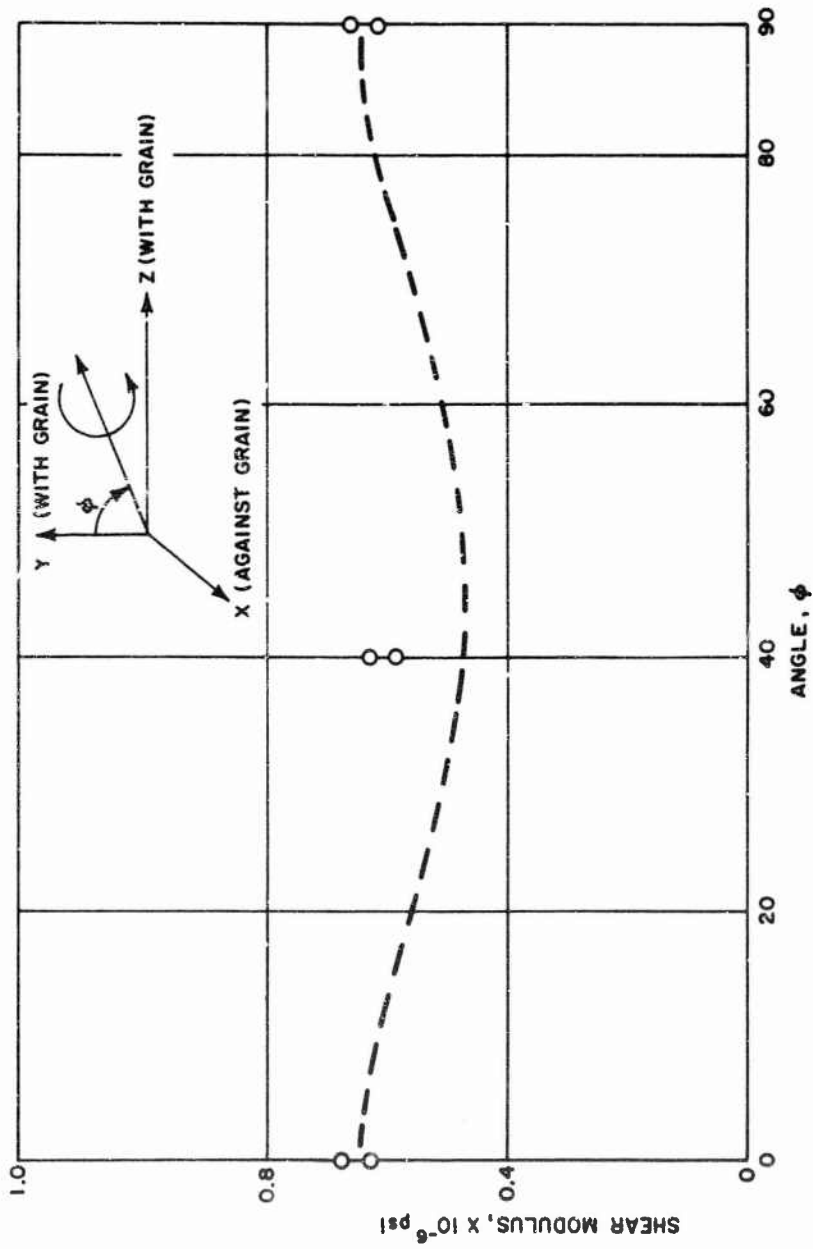
One of the goals of this research, as mentioned earlier, was to obtain an empirical NDT parameter for assessing the resistance of graphite material to thermal shock. It has been demonstrated that the graphite behaves as an anisotropic medium. Therefore, in order to design meaningful experiments to formulate a more rational theoretical basis for the associated NDT measurements, thermoelastic stress wave phenomena must be understood. A detailed presentation of the equation of wave propagation in transversely isotropic media appears in the appendix. This full set of field equations must be resorted to in order to determine the importance of coupled thermo-mechanical behavior.

For most isotropic elastic material, the coupling effects in the thermoelastic field equations are justifiably negligible. However, for graphites, the order of magnitude of the coefficients of the equations has not been completely defined over a wide temperature range and so the importance of the coupling terms is somewhat unsettled.



760341D

Figure 13 THEORETICAL UNIAXIAL MODULUS VARIATION



760342 D

Figure 1.4 THEORETICAL AND OBSERVED SHEAR MODULUS VARIATIONS

Beyond these matters, complexities associated with heat conduction in which the body undergoes a phase change during exposure to the thermal environment undoubtedly are important in relation to thermal shock phenomena. These reasons all add credence to the statement that full-scale performance of rocket nozzles cannot be predicted from ordinary properties data. However, this is only in part true since the refinements of more sophisticated mathematical representations have not been applied. Admittedly, even the asymptotic solutions to these problems are difficult, time consuming and costly. Rocket nozzle failures, however, are also costly and dangerous as well.

The failure response of isotropic materials can be considered from both the microscopic and macroscopic point of view. From the viewpoint of gross engineering types of response, it is useful to enumerate the ordinarily used fracture criteria for elastic media.

1. maximum principal stress
2. maximum principal strain
3. maximum principal stress difference (shear stress)
4. maximum principal strain difference (shear strain)
5. maximum distortional strain energy
6. maximum conserved distortional strain energy
7. maximum total strain energy

The important point to note is that no universal fracture criterion has been established and that the success of a given fracture hypothesis depends in large measure upon the material with which it is associated.

One can quickly list the various yield criteria and attempt to verify the applicability of these theories to graphite behavior. For example, the VonMises yield criterion based on the mean value of the principal stress difference takes the form

$$\sqrt{2} \sigma_0 = \sqrt{(\sigma_1 - \sigma_2)^2 + (\sigma_2 - \sigma_3)^2 + (\sigma_3 - \sigma_1)^2} \quad (11)$$

for simple tension this equation results in σ_0 , while for pure shear, the yield stress = $\sigma_0/\sqrt{3}$. In graphites, the shear strength is of the same magnitude as the tensile strength which negates such simple criterion.

Hill⁽¹¹⁾ postulated that the yield condition for anisotropic media is a quadratic function of the stress components

$$2f(\sigma_{ij}) = F(\sigma_2 - \sigma_3)^2 + G(\sigma_3 - \sigma_1)^2 + H(\sigma_1 - \sigma_2)^2 + 2L\tau_{23}^2 + 2M\tau_{31}^2 + 2N\tau_{12}^2 \quad (12)$$

where X_1, X_2, X_3 are axes of material symmetry and $F, G, H, L, M,$ and N are material constants.

The strength of quasi-homogeneous anisotropic composites was reported by Azzi and Tsai⁽¹²⁾. One of the basic assumptions of their failure condition is that there exist three mutually perpendicular planes of symmetry within the anisotropic body and the material is, therefore, taken to be orthotropic strengthwise. Under this assumption the coordinate system for the state of stress and the material symmetry must be the same. Thus, the state of stress imposed on a body must be transformed to the coordinate system of material symmetry and then the yield conditions applied. For uniaxial ultimate strength, Tsai has suggested that the applicable equation is

$$\sigma_1' = \sigma_1 \left[\cos^4 \phi + \left\{ \left(\frac{\sigma_1}{r} \right)^2 - 1 \right\} \cos^2 \phi \sin^2 \phi + \left(\frac{\sigma_1}{\sigma_2} \right)^2 \sin^4 \phi \right]^{1/2} \quad (13)$$

The appropriateness of such an equation for graphite materials has not been investigated. However, an alternate equation may be derived for the case of pure shear (see Reference 13, page 12). For the case where $\phi = 45^\circ$, the shear strength takes the form

$$r' = \sigma_1 \sqrt{\left(\frac{\sigma_1}{\sigma_2} \right)^2 + 2} \quad (14)$$

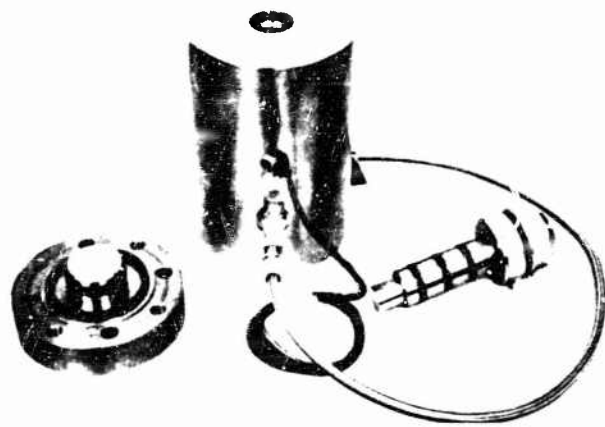
which reduces to $\sigma_0/\sqrt{3}$ when $\sigma_1 = \sigma_2$ and therefore, agrees with the Von Mises condition. The applicability of this equation for predicting shear strength can be assessed by using the data of Table II as well as that available in the literature^(9, 10).

Considering the lack of success of simple yield criterion, and the fact that correlations with nondestructive tests can be established between modulus, strength and porosity of graphite, it is suggested that a more realistic yield criterion might be the Mohr Coulomb theory ordinarily applied to granular materials. This is particularly true since in small solid propellant rocket engines applications the nozzle insert is in part subjected to a hydrostatic compression.

The failure condition can be stated in the form

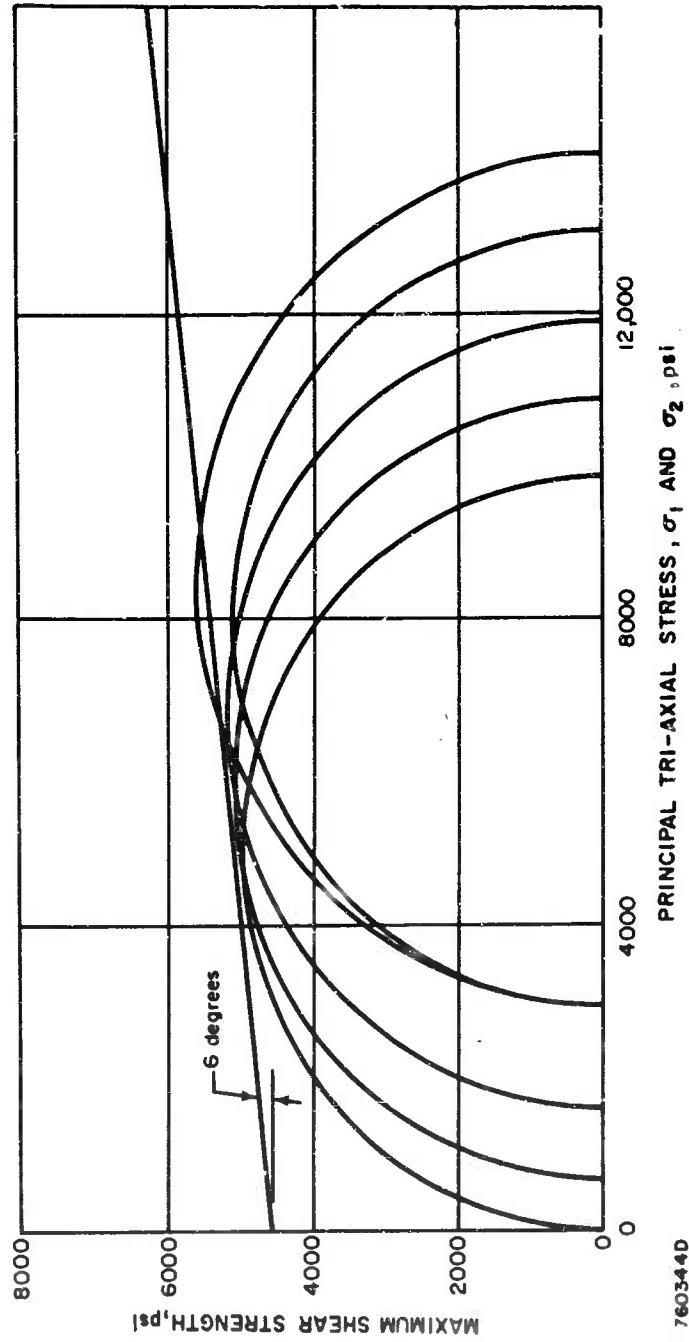
$$\tau_{\max} = k + \sigma_n \tan \phi \quad (15)$$

and the proof of such behavior can be established by performing triaxial tests on cylinders of the material. For this purpose, the apparatus illustrated in Figure 15 was used to subject membrane covered molded ATJ graphite to several levels of hydrostatic pressure and then to compress the sample to failure with the axial loading piston. A detailed discussion of routine and special triaxial test techniques appears in Reference 14. For the ATJ specimens, the experiments were performed on both with and against the grain orientations and the results are presented in Figures 16 and 17.



750343D

Figure 15 HIGH PRESSURE TRIAXIAL TEST APPARATUS



760344D

Figure 16 MOHR COULOMB YIELD ENVELOPE ATJ GRAPHITE WITH THE GRAIN

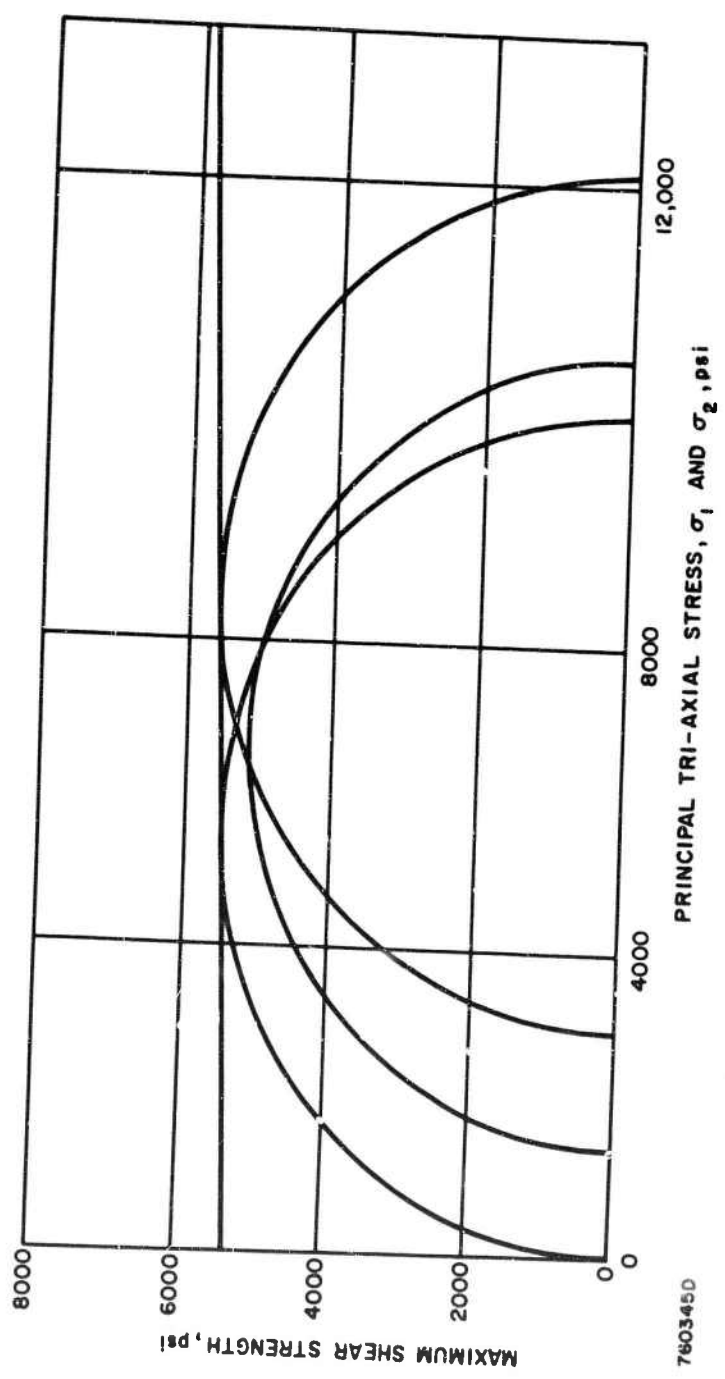


Figure 17 MOHR COULOMB YIELD ENVELOPE ATJ GRAPHITE AGAINST THE GRAIN

These yield envelopes show that the with the grain orientation has significant hydrostatic pressure effects on the maximum shear strength while only very slight influences were evident for the against the grain orientation. This suggests that the with grain orientation exhibits response characteristics similar to granular media.

In order to evaluate the influence of this yield phenomena a simple plasticity problem is now considered by comparison of elementary and Mohr Coulomb criteria for the case of a rigid plastic wedge. The solutions for this case with uniform normal pressure on one face are compared for each. (see Figure 18)

Reference 15 lists the solution for the simple yield criteria as

$$p = 2k (1 + 2 \beta_0 - 90^\circ) \quad (16)$$

while for the case of the Mohr Coulomb Criteria, Sokolovsky⁽¹⁶⁾ suggests substituting the equations

$$\begin{aligned} \tau_{\max} &= k + \sigma_n \tan \phi \\ \sigma_n &= \frac{1}{2} (\sigma_1 + \sigma_2) - \left(\frac{\sigma_1 - \sigma_2}{2} \right) \sin \phi \end{aligned} \quad (17)$$

into the yield criterion $F(\sigma_{ij})$ so that one has

$$\left[k \cos \phi + \frac{1}{2} (\sigma_1 + \sigma_2) \sin \phi - \frac{1}{2} (\sigma_1 - \sigma_2) \cos^2 \phi - \frac{1}{2} (\sigma_1 - \sigma_2) \sin^2 \phi \right] \quad (18)$$

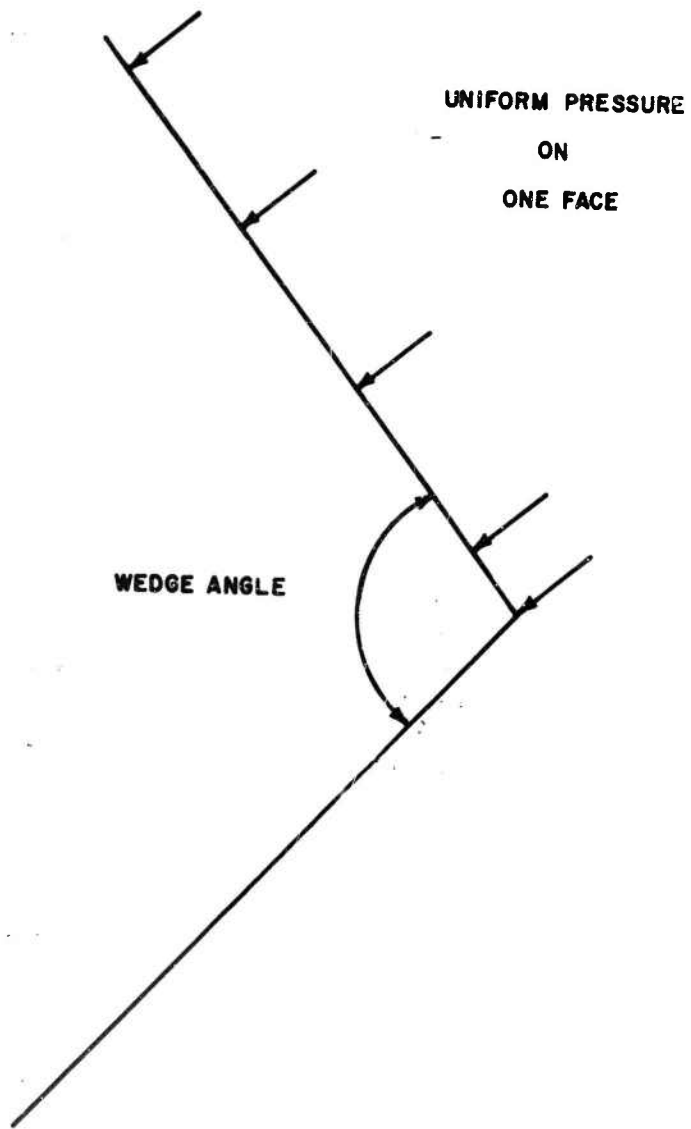
Satisfying the equilibrium equations then leads to the expression for the limiting plastic pressure on the wedge

$$p' = k \cot \phi \left[\exp \{ (2\beta_0 - \pi) \tan \phi \} \tan^2 \left(\frac{\pi}{4} + \frac{\phi}{2} \right) - 1 \right] \quad (19)$$

$$2\beta_0 > \frac{\pi}{2}$$

The ratio of p'/p determined using equations 16 and 17 where k and ϕ are obtained from Figure 16, are compared in Figure 19 as a function of wedge angle. The solution of course is not valid for angles approaching 180° since this geometry would lead to a problem of contained plasticity. In the range of 90° to 140° , the observed ratio shows a variation of 20 to 30%.

It is suggested that the Mohr Coulomb Criteria is mathematically tractable and is perhaps a more realistic description of failure of the graphite under certain conditions.



760349D

Figure 10 SKETCH OF LOADED WEDGE

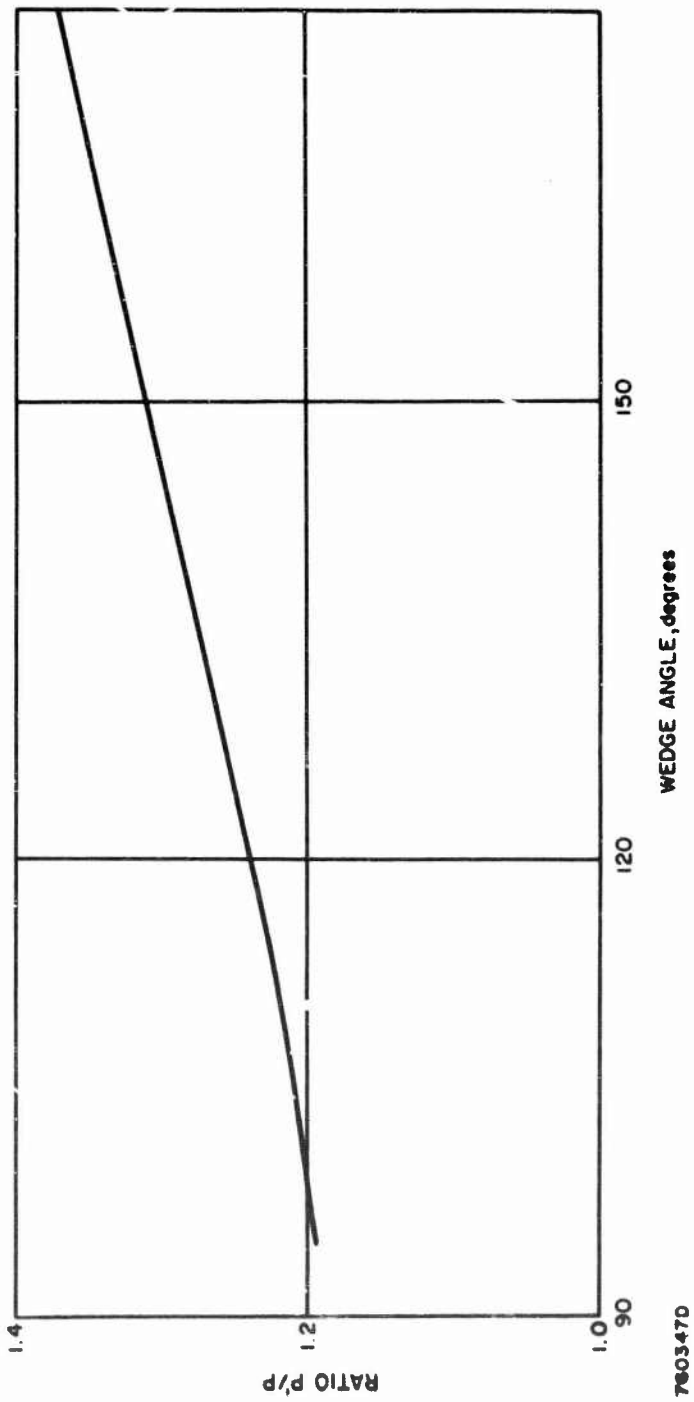


Figure 19 COMPARISON OF MAXIMUM PRESSURE AS A FUNCTION OF WEDGE ANGLE FOR SIMPLE VERSUS MOHR COULOMB YIELD CRITERION

7603470

E. Investigation of Infrared Techniques for Nondestructive Determination of Thermal Conductivity

The thermal conductivity of materials is an important physical quantity to the engineer involved in the design of fabrications requiring heat transfer consideration. Conductivity is a basic quantity that is absolutely necessary for determining the amount of heat that can flow in a material continuously. When combined with values of the density and heat capacity of a material the conductivity is proportional to a thermal parameter called diffusivity, by which the spatial intensity and temporal distribution of thermal transients in the material can be determined. When conductivity is combined with knowledge of a material's elastic modulus, tensile strength and expansion coefficient, the relative ability of high-temperature refractories, such as graphite, to withstand thermal shock can also be determined.

Determination of a material's thermal conductivity has been traditionally performed under steady-state conditions of heat flow on specimens having some experimentally suitable geometry. Some recent studies have described the use of a transient heating through transmission technique to determine conductivity, diffusivity and heat capacity^(17, 18, 19). These studies also have required the use of special specimen geometries and the need for access to two opposite surfaces, both of which necessitate the destructive testing of a fabrication. These technique requirements result principally from limitations imposed in attempting to experimentally achieve boundary conditions suitable for analysis.

Indirect nondestructive testing techniques for determining thermal conductivity in many electrical conductors are feasible by correlating their electrical and thermal conductivities. Electrical measurements, however, can usually be performed only on large sections and result in bulk determinations. For other materials, such as dielectrics and graphite, suitable correlations between their thermal conductivities and other physical quantities have not been established as yet. Nondestructive direct measurements, then, must be performed especially on these latter materials, and preferably in a practical manner that yields results in a comparatively localized region, in order to observe maximum material variability and contributing processes.

It is believed that prior to this study the direct nondestructive determination of the thermal conductivity of fabrications has not been performed. To this end, a novel technique has been developed from which the near-room-temperature conductivity of a solid can be determined directly. Theory is presented and is supported by limited experimentation to indicate the feasibility of the technique. The technique is simple and consists of simultaneously heating a surface of a "semi-infinite" solid by radiation and observing the temperature history at this surface using an infrared radiometer as the radiance sensor. Analysis of the history record by comparison with a standard record and knowledge of the unknown's density and specific heat permits the determination of the conductivity.

Type ATJ graphite was the material selected for emphasis in this study because of Avco's present interest in it, stemming from its range of properties variability. There is every reason to believe, however, that the technique can be extended to include testing of solids in general.

1. Theory

The following theoretical development is aimed at obtaining the thermal conductivity of a solid by observing the temperature history of an exposed surface, using an infrared radiometer, while this surface is subjected to a constant radiant heat flux. By comparing geometrical characteristics of this history with that for a solid having a known conductivity, together with knowledge of the unknown's density and heat capacity, the unknown conductivity may be determined. This transient technique does not require knowledge of the flux incident to the surface, which is a most desirable consequence. For validity, however, it does require adherence to certain boundary conditions and to criteria for nondestructive testing and observability of the history recording.

2. Experimental Parameters

a. Fundamentals of Heating Method

Three criteria are used as bases in this development. The first criterion presumes the solid to be dimensionally large enough so that it appears semi-infinite to heat flow during the period of simultaneous heating-observation. If it is assumed that the heat flow front is spatially uniform in intensity and is unidirectional, so that no lateral heat flow loss occurs, this criterion is satisfied for the thickness dimension by the condition⁽²⁰⁾

$$L_{\infty} \geq (3\alpha t)^{1/2}, \quad (20)$$

where L_{∞} is the distance into the solid beyond which semi-infiniteness exists, α is thermal diffusivity, and t is time.

The second criterion presumes that the temperature history of the solid's surface is of parabolic form and is generated by the following relationship⁽²¹⁾

$$T(Q, t) - T_0 = \frac{2Q}{k} \left(\frac{\alpha t}{\pi} \right)^{1/2} \quad (21)$$

where T is the temperature of the surface above an initial ambient temperature T_0 , Q is the heat flux per unit area per unit time absorbed at the surface, and k is thermal conductivity. The diffusivity is defined

in terms of k , the density ρ , and the heat capacity at constant pressure, C_p , as

$$a = \frac{k}{\rho C_p} \quad (22)$$

The third criterion presumes that the surface temperature of the solid rises no more than about 10 degrees Centigrade during the period of heating so that the modified Stephan-Boltzmann law

$$W = \frac{1}{\pi} \epsilon_T \sigma (T^4 - T_0^4), \quad (23)$$

which describes the rate of heat loss from a body at T to a body at T_0 , can be approximated by the relationship

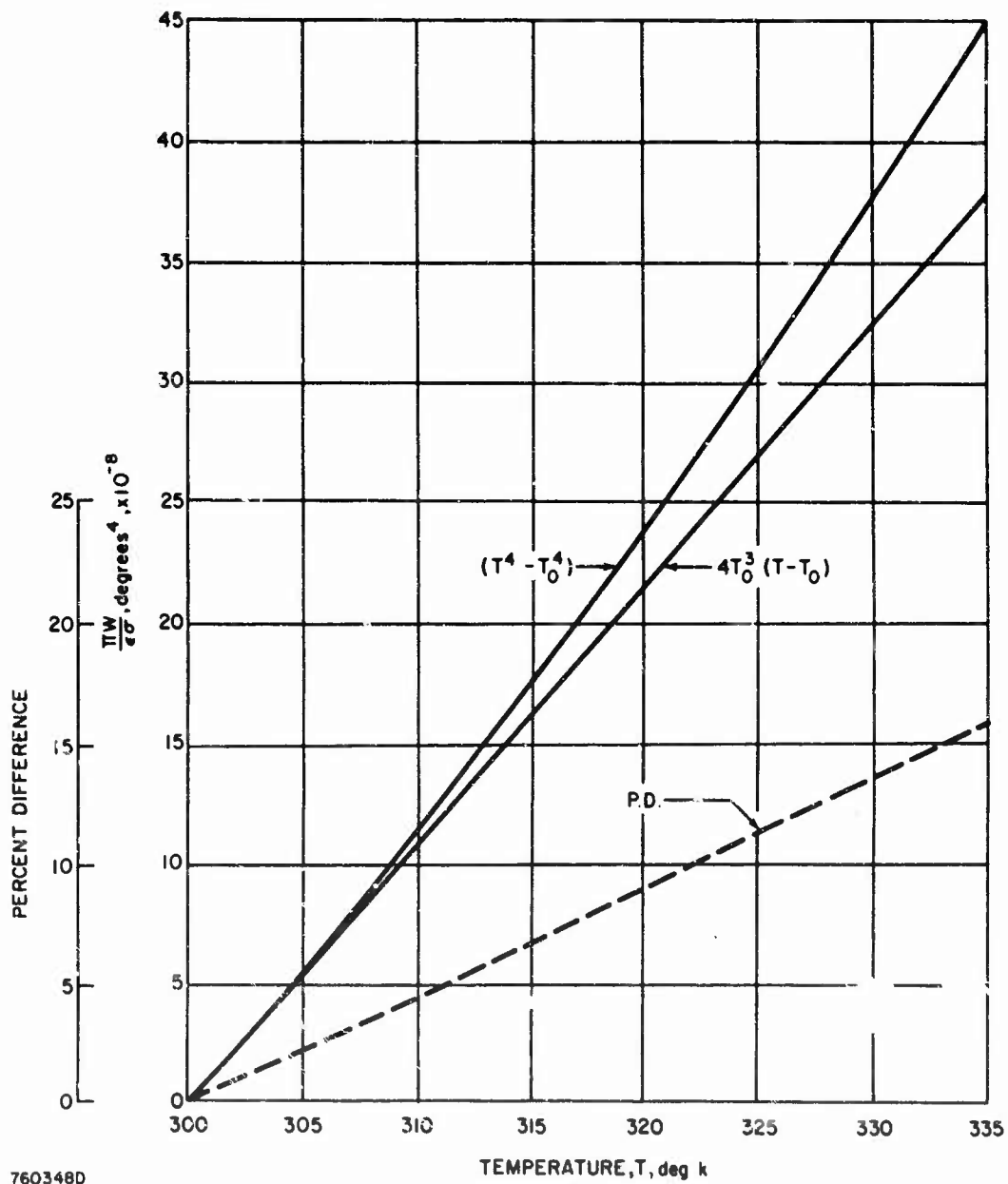
$$W \approx \frac{4}{\pi} \epsilon_T \sigma T_0^3 (T - T_0). \quad (24)$$

In Equations (23) and (24) W is the radiant energy or radiance emitted from the surface, assuming a cosine or Lambert law distribution, ϵ_T is the total radiant emissivity of the surface, and σ is the Stephan-Boltzmann constant. These two equations are plotted in Figure 19, from which it is seen that a 10 degree C rise in the temperature of a surface initially at 27 degree C results in a 4 percent difference between the theoretical and approximate forms of the radiation laws. For most solids, this 10 degree C rise above ambient will cause no significant change in their physical properties, so that testing is indeed nondestructive.

Since a radiometer is used to detect the surface temperature, the radiant energy entering the radiometer is converted into an electrical voltage, V , such that

$$V = K W' \quad (25)$$

where K is a constant that accounts for this conversion, and $W' = \frac{4}{\pi} \epsilon_T \sigma T_0'^3 (T - T_0')$ where T_0' is the radiometer's reference source temperature. The difference between T_0' and T_0 is a constant temperature δ . Thus the temperature history curve is actually one of voltage vs. time.



760348D

Figure 20 THEORETICAL VERSUS APPROXIMATE FORM RADIATION LAWS

Lastly, in this basis of development, Q is the flux of heat deposited at the solid's surface from the radiation source which emits a flux F incident to the surface. These two quantities are related by the equation

$$Q = a_T F, \quad (26)$$

where a_T is the total radiant absorptance of the surface. For opaque gray surfaces, $\epsilon_T = a_T$. Furthermore, since heating of the surface is due principally to that part of the incident radiation energy spectrum in the infrared wavelength region, as is the energy spectrum emitted by the heated solid, then both spectra correspond to the spectral region detected by the radiometer, so that $\epsilon_T = \epsilon_\lambda$, where ϵ_λ is the emissivity of the radiometer's detectible infrared spectrum.

Combining Equations (21, 22, 24-26) and solving for V yields the relationship

$$V = A \left(\frac{\epsilon_\lambda^4}{k \rho C_p} \right)^{1/2} t^{1/2} - B, \quad (27a)$$

where

$$A = \frac{8KF\sigma T_o'^3}{\pi^{3/2}} \quad (27b)$$

$$B = \frac{4K\epsilon_\lambda\sigma T_o'^3\delta}{\pi}, \quad (27c)$$

$$V' = \frac{V+B}{A} \quad (27d)$$

Equation (27a) is a voltage history of parabolic form corresponding to the surface temperature history. The constants A and B are independent of any characteristics of the solid. The latus rectum of the parabola equals

$\frac{A^2 \epsilon_\lambda^4}{k \rho C_p}$, so that the shape of the history curve is dependent on the flux, F ,

the emissivity, ϵ_λ , and the quantity $(k \rho C_p)$. A higher flux, or emissivity, or a lower conductivity increases the signal voltage and the width of the parabola.

temperature through a figure of merit of the radiometer called NET. * The NET is the temperature, seen by the radiometer's field of view, required to obtain a $\Sigma = 1$. NET has units of degrees Centigrade, where small values indicate high radiometer sensitivity and performance. The NET for the radiometer, as used in these studies, was 0.5 degree C, at a reference temperature of 300 degree K.

c. Minimum Radiation Flux

By combining Equations (27) and (34), it is possible to obtain a relationship for the minimum incident radiation flux, F_0 , necessary to obtain an observable radiometer signal voltage within the response time of the source-detector-recorder system. This relationship is

$$F_0 \text{ (cal./cm}^2\text{-sec)} = \frac{\pi^{1/2}}{2} \frac{(k\rho C_p)^{1/2}}{\epsilon_\lambda^2 \tau^{1/2}} \left[\frac{\pi V_0}{\left(1 - \frac{1}{\Sigma^2}\right)^{1/2} K \sigma T_0^3} + \epsilon_\lambda \delta \right]$$

Values of the parameters for the radiometer used in this study are:

$$\begin{aligned} V_0 &= 0.002 \text{ v. lts (rms)} \\ K &= 26.7 \text{ volts - cm}^2\text{-sec. /cal.} \\ T_0' &= 304^\circ \text{ K} \\ \delta &= 4^\circ \text{ K} \\ \sigma &= 1.37 \times 10^{-12} \text{ cal. /cm}^2\text{-sec. -}^\circ \text{ K}^4. \end{aligned}$$

A signal-to-noise ratio $\Sigma = 3$ will be assumed. Graphite and copper are two solids considered and both are presumed to be coated, each having an emissivity value, ϵ_λ , equal to 0.85. The quantities $(k\rho C_p)$ are calculated from published data for k , ρ , and C_p , which are tabulated in Table I, and are 0.82 and 0.081 cal.²/cm⁴-sec.²-°K² for copper and graphite (in a direction with the grain), respectively. Substitution of these values into Equation (35) reduces it to

$$F_0 = 11.9 \frac{(k\rho C_p)^{1/2}}{\tau^{1/2}} \quad (36)$$

For copper and graphite and for a system response time equal to 80 msec, Equation (36) yields

$$\begin{aligned} F_{0\text{cu}} &= 37.7 \text{ cal./cm}^2\text{-sec} \\ &= 161 \text{ watts/cm}^2 \\ F_{0\text{G}} &= 11.8 \text{ cal./cm}^2\text{-sec} \\ &= 49 \text{ watts/cm}^2 \end{aligned}$$

*NET is defined as the temperature difference required to produce an rms signal voltage equal to the noise voltage, V_N , in a 1 cps bandwidth for a stated temperature in the field of view of the radiometer.

It is fortunate that C_p is constant for this case, since the densities can be readily determined using, for example, a nondestructive testing gamma-ray radiometric density-gauging technique, or an ultrasonic velocity technique.

b. Observation Sensitivity

1.) Reflected Radiation

All surfaces reflect radiation to some degree, so that $r_\lambda > 0$. This creates a problem experimentally. During heating a part of the radiant energy incident to the solid's surface is reflected into the optics of the radiometer. The total radiation sensed by the radiometer is composed of this reflected radiation and the solid's self-emitted radiation. If r_λ is independent of temperature, the reflected component is constant during heating. This effect can be stated mathematically as

$$V'' = V + V_R \quad (33)$$

where V is the self-emitted signal voltage described by Equation (27), and V_R is the signal voltage caused by the reflected radiation. It is to be noted that $\tan \theta$, from Equation (28), is not affected by V_R since it depends on voltage differences. To observe the parabolic-shaped informational signal voltage, which rides on top of V_R , the voltage difference, $V'' - V_R$, must be greater than the discrimination level of the radiometer. If F and/or ϵ_λ is too small, or k too large, such that $V'' - V_R$ cannot be observed, then the heating curve will appear almost square in shape, but with slightly canted skirts. These skirts are a consequence of both the finite response speed of the radiometer's detector and the pulse rise time of the radiation incident to the surface. Of course, if V_R can be suppressed electronically in the radiometer and sensitivity can be increased to observe just V , reflection is not a problem.

2 Signal-to-Noise Ratio (Noise Equivalent Temperature)

This increase in sensitivity may introduce another discrimination problem, which involves both the noise equivalent temperature (NET) of the radiometer and the criterion of acceptable signal-to-noise ratio, Σ , for observability. The observable signal voltage, V_o , is related to Σ by the expression

$$V_o = V_N (\Sigma^2 - 1)^{1/2}, \quad (34)$$

where $\Sigma = V/V_N$ and V_N is the noise voltage. If $\Sigma = 1$, then $V_o = 0$ and an informational signal cannot be observed. Thus Σ must be greater than unity as one criterion for detectability. Values of $\Sigma \geq 3$ indicate easily observable informational signals. Furthermore, V_N can be related to

temperature through a figure of merit of the radiometer called NET.* The NET is the temperature, seen by the radiometer's field of view, required to obtain a $\Sigma = 1$. NET has units of degrees Centigrade, where small values indicate high radiometer sensitivity and performance. The NET for the radiometer, as used in these studies, was 0.5 degree C, at a reference temperature of 300 degree K.

c. Minimum Radiation Flux

By combining Equations (27) and (34), it is possible to obtain a relationship for the minimum incident radiation flux, F_0 , necessary to obtain an observable radiometer signal voltage within the response time of the source-detector-recorder system. This relationship is

$$F_0 \text{ (cal./cm}^2\text{-sec)} = \frac{\pi^{1/2}}{2} \frac{(k\rho C_p)^{1/2}}{\epsilon_\lambda^2 \epsilon^{1/2}} \left[\frac{\pi V_0}{\left(1 - \frac{1}{\Sigma^2}\right)^{1/2} K \sigma T_0^3} + \epsilon_\lambda \delta \right]$$

Values of the parameters for the radiometer used in this study are:

$$\begin{aligned} V_0 &= 0.002 \text{ volts (rms)} \\ K &= 26.7 \text{ volts - cm}^2\text{-sec./cal.} \\ T_0' &= 304^\circ \text{K} \\ \delta &= 4^\circ \text{K} \\ \sigma &= 1.37 \times 10^{-12} \text{ cal./cm}^2\text{-sec. - }^\circ \text{K}^4. \end{aligned}$$

A signal-to-noise ratio $\Sigma = 3$ will be assumed. Graphite and copper are two solids considered and both are presumed to be coated, each having an emissivity value, ϵ_λ , equal to 0.85. The quantities $(k\rho C_p)$ are calculated from published data for k , ρ , and C_p , which are tabulated in Table I, and are 0.82 and 0.081 cal.²/cm⁴-sec.²-°K² for copper and graphite (in a direction with the grain), respectively. Substitution of these values into Equation (35) reduces it to

$$F_0 = 11.9 \frac{(k\rho C_p)^{1/2}}{\epsilon^{1/2}} \quad (36)$$

For copper and graphite and for a system response time equal to 80 msec, Equation (36) yields

$$\begin{aligned} F_{0\text{cu}} &= 37.7 \text{ cal./cm}^2\text{-sec} \\ &= 161 \text{ watts/cm}^2 \\ F_{0\text{G}} &= 11.8 \text{ cal./cm}^2\text{-sec} \\ &= 49 \text{ watts/cm}^2 \end{aligned}$$

*NET is defined as the temperature difference required to produce an rms signal voltage equal to the noise voltage, V_N , in a 1 cps bandwidth for a stated temperature in the field of view of the radiometer.

TABLE I. Published values of ρ , Cp, and k, and calculated values of α and ($k\rho Cp$) for copper, aluminum, Type 10-20 steel, lead, and Type ATJ graphite.

Material	Density ρ (gm/mm)	Heat Capacity Cp (cal./gm-°C)	Thermal Cond. k (cal./cm-sec-°C)	Thermal Diffusivity α (cm ² /sec)	$k\rho Cp$ (cal ² /m ⁴ -sec.-°C)
Copper	8.9	0.10	0.92	1.03	0.82
Aluminum	2.7	0.22	0.49	0.83	0.29
Steel (Type 1020)	7.8	0.11	0.11	0.13	0.10
Lead (Chemical Grade)	11.3	0.035	0.08	0.20	0.032
Graphite (Type ATJ <u>with grain</u>)	1.7	0.17	0.28	0.97	0.081
Graphite (Type ATJ <u>against grain</u>)	1.7	0.17	0.21	0.73	0.061

That is to say, 161 watts/cm² of infrared radiation incident to the surface of copper, which has an infrared emissivity of 0.85, is necessary to raise the temperature of the surface by an amount sufficient for observation with a signal-to-noise ratio of 3, after a period of 80 msec. has elapsed from pulse initiation. Similarly, 49 watts/cm² are necessary when studying graphite oriented in a direction with the grain. These values for F₀ are reasonable when compared with the radiation source actually used in this study. It must be remarked that those results have validity only when: (1) the solid appears semi-infinite in thickness during the observation period; (2) the incident radiation is uniform in intensity over the surface; (3) heat flow within the solid is unidirectional and perpendicular to the surface; and (4) the radiometer's field-of-view on the surface is located such that the region of observation experiences the three foregoing boundary conditions.

d. Effect of Coatings

1.) Emissivity

The effect of those coatings which produce an emissivity change at the solid's surface on the radiation flux requirement can be determined from Equation (35) by differentiating it with respect to ϵ_λ and solving for the relative flux change $\Delta F_0/F_0$. This yields the expression:

$$\frac{\Delta F_0}{F_0} = - \left(\frac{2D + E \epsilon_\lambda}{D + E \epsilon_\lambda} \right) \frac{\Delta \epsilon_\lambda}{\epsilon_\lambda} \quad (37a)$$

where

$$\frac{D}{E} = \frac{\pi V_0}{\left(1 - \frac{1}{\Sigma^2}\right)^{1/2} \sigma K T_0^3 \delta} \quad (37b)$$

The minus sign in (a) indicates that a decrease in emissivity requires an increase in the flux requirement to produce an observable signal. Substitution of the radiometer and S/N parameters listed above into Equation (37b) gives the value $D/E \approx 1.5$, so that Equation (37b) reduces to:

$$\frac{\Delta F_0}{F_0} \approx - \frac{(\epsilon_\lambda + 3)}{(\epsilon_\lambda + 1.5)} \frac{\Delta \epsilon_\lambda}{\epsilon_\lambda} \quad (38)$$

One example of the use of Equation (38) is to consider a 5 percent decrease in ϵ_λ at an $\epsilon_\lambda = 0.85$. This emissivity change requires a corresponding increase in F_0 of 6.7 percent. Similarly, a 5 percent increase in ϵ_λ at $\epsilon_\lambda = 0.1$ indicates that F_0 can be diminished by 9.7 percent.

2.) Pulse Retardation

Since the solids considered in this study are good thermal conductors, the effect of a poor conducting coating, such as a lacquer, having a thickness as small as 10^{-4} cm, is to initially retard the flow of heat into the solid(23). As a consequence of this retardation, the surface temperature is somewhat greater during the first few seconds after pulse initiation compared to the temperature that would result from an ideal coating having the same emissivity but an infinite surface conductance. If the same coating is applied to solids having different conductivities, the rate of temperature rise will be greater the lower the conductivity of the solid. Thus, the tangent of the angle of temperature rise, in Equation(28b) will be somewhat greater the poorer the solid conductor. For example, since graphite has a lower conductivity than copper, the ratio of tangents, $\frac{\tan \theta \text{ (graphite)}}{\tan \theta \text{ (copper)}}$

will be less for a coating of finite conductance than for the ideal case of infinite surface conductance. Similarly, the ratio $\frac{(k\rho C_p) \text{ (copper)}}{(k\rho C_p) \text{ (graphite)}}$

will be less than for the ideal case. Moreover, for lacquer-coated graphite, the ratio $\frac{k \text{ (with the grain)}}{k \text{ (against the grain)}}$ will also be less than for the ideal case.

e. History Curve Analysis

The voltage histories for the several solids studied have been calculated using Equation(27) and the published data listed in Table I, and are plotted in Figure 21. The slopes have been constructed for a one second time increment between 1.3 and 2.3 seconds. As long as this increment is the same and is chosen at the same time, the ratio of slopes, $\frac{\tan \theta \text{ a}}{\tan \theta \text{ b}}$, remains constant, as

indicated by Equation (29). The time increment can be selected between 0 and a time t_1 , of course, but this requires knowledge of the location of the history curve's vertex, which is difficult to determine experimentally due to the response time of the system. Selection of the time increment is not entirely arbitrary, however, since consideration must be given to the criterion that the solid appear semi-infinite in thickness during heating, as satisfied by Equation(20). This thickness limitation, L_∞ , has been calculated from published data at a time equal to 2 seconds and is listed in Table II for each of the solids studied. It is seen that specimens having approximately a one-inch thickness, which is experimentally convenient, appear semi-infinite during a 2 second observation period. Observation for periods greater than this will result in a departure from the history curve's parabolic shape after 2 seconds.

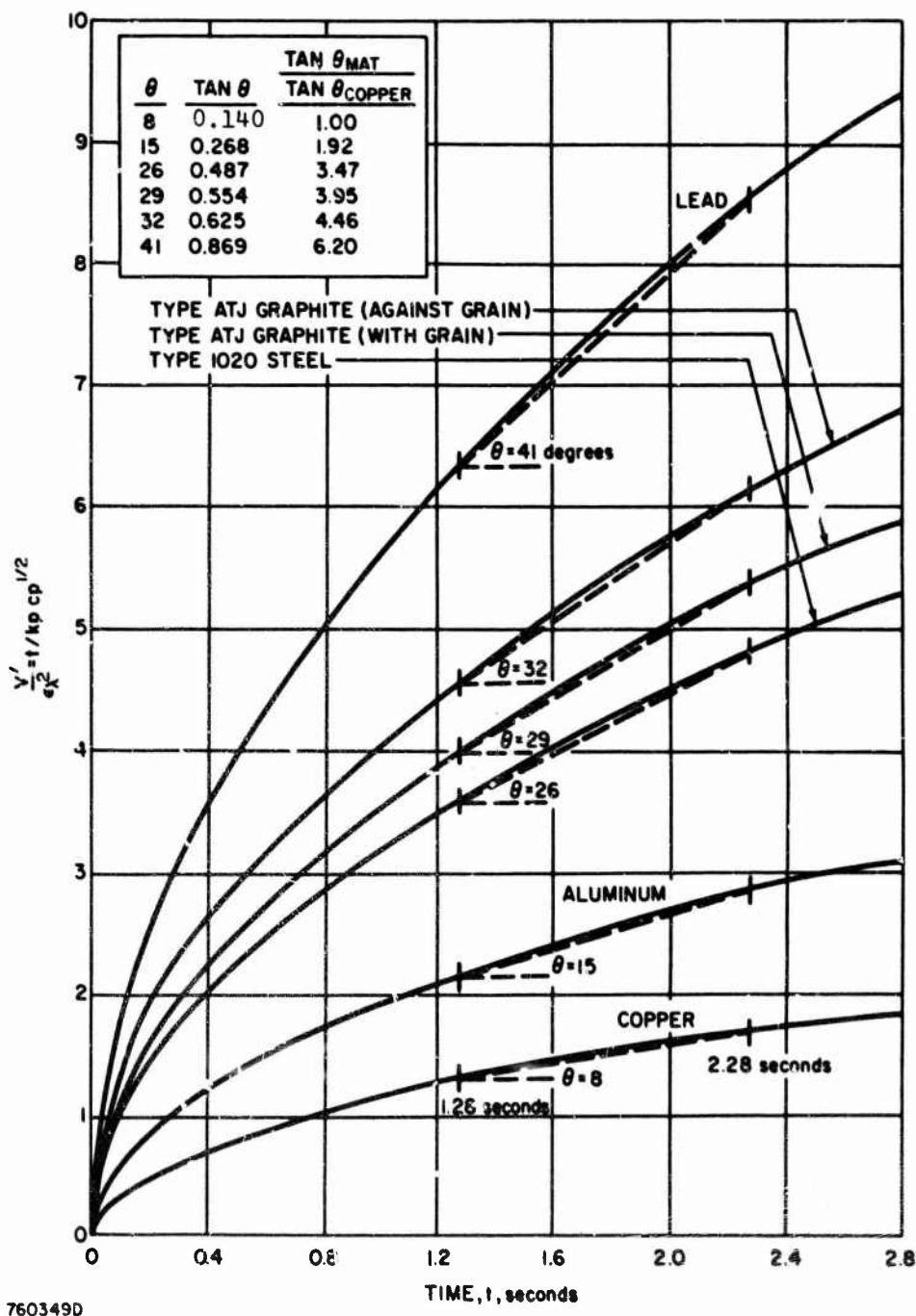


Figure 21 TIME-TEMPERATURE HISTORIES OF MATERIALS

TABLE II. Material thicknesses for which specimens are considered semi-infinite in extent.*

Material	$3 at^{**}$ ($t = 2$ secs.)	Thickness L (inches) $= (3 at)^{1/2}$
Copper	6.18	0.98
Aluminum	4.98	0.88
Steel (Type 1020)	0.78	0.35
Lead (Chemical Grade)	1.20	0.47
Graphite (Type ATJ <u>with grain</u>)	5.82	0.95
Graphite (Type ATJ <u>against grain</u>)	4.38	0.82

* A material is considered semi-infinite to the flow of heat when the condition, $L \leq L_{\infty} = (3 dt)^{1/2}$, obtains.⁽⁴⁾

** The thermal diffusivities used in this calculation are obtained from the published data listed in Table I. Although the experimental heating time, t , was 3 seconds, the time of interest in the calculations is approximately 1 to 2 seconds.

It must be remarked that the family of curves in Figure 21 indicate only the relative displacements of each curve. The group will appear steeper the greater the incident radiation flux and/or emissivity, and will appear flatter the smaller the flux and/or emissivity. If the flux is less than the critical quantity, F_0 , in Equation(35), during the heating period then observation of a heating curve is not possible.

f. Cooling Method

Another approach for obtaining thermal conductivity using a comparative technique, along similar lines as described, requires radiometric observation of the solid's surface while it cools after heating. This approach is workable, but is not as practical as the heating method. Analogous to Equation(21) for the temperature history during heating, is the following equation, which generates the cooling history at the solid's surface (24)

$$T(Q, t) - T_0 = \frac{2Q}{k} \left(\frac{a}{\pi} \right)^{1/2} [t^{1/2} - (t - \tau)^{1/2}] \quad (39)$$

where τ is the heat pulse duration. For solution, t must be greater than τ . If $t = \tau$, then Equation(21) results. Equation (39), then, generates a curve which is the difference between two parabolas having the same latus rectums but separated in time by τ , even though reflection exists during heating. The chief advantage of the cooling method compared to the heating method is that reflected radiation no longer requires discrimination in the experiment. However, sensitivity and signal-to-noise ratio must still be considered for observability, and therefore, the detector and recorder must either be protected against overshooting from the reflected radiation component if monitoring is continuous, or they must be activated immediately following the termination of the heat pulse.

One serious limitation of the cooling method is due to the requirement that the solid must appear semi-infinite during both the heating and cooling cycles up to the time observation is complete. Thus, the heating pulse duration and the duration of observation while the solid cools together must be less than the time for transport of the pulse through the body. For most good conductors, this can only be accomplished by depositing a sufficient quantity of energy uniformly over a suitable region on the solid's surface, within a short interval, so that excessive temperatures are not attained, and then observing the cooling curve up to the semi-infinite time limitation. This might be accomplished using a laser as a radiation source, which has the advantage of emitting radiation in other than the infrared region, so that reflection is not a problem. Analysis of the cooling curve to obtain a tangent ratio, from which a conductivity ratio is determined, will be similar to that for the heating curve. Other than for the reflection problem, the cooling method offers no advantage over the heating method and, in general, probably would prove to be more critical to use and would require a more costly radiation source.

3. Experiment

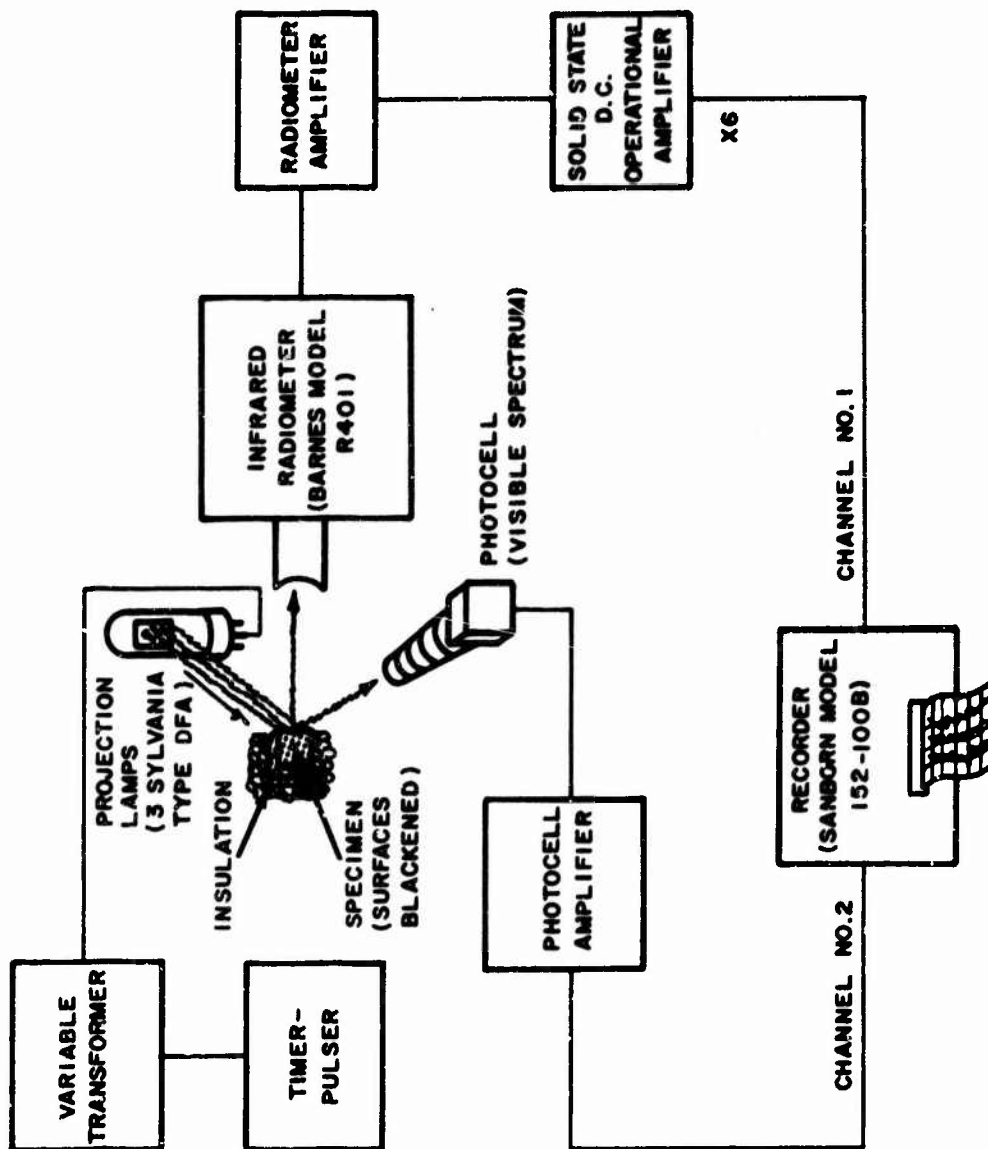
Measurements were performed on five planar-oriented type ATJ graphite specimens exhibiting a range of densities and four types of good thermal conductors, having a broad range of thermal properties and characteristics, and densities. These good conductors were: (1) drawn copper; (2) drawn aluminum; (3) type 1020 drawn steel; and (4) chemical grade cast lead. Published values of their properties, from which calculated quantities of interest are obtained, are listed in Tables I and II. The purpose of selecting these materials was to determine the range of validity of the technique for solids having conductivities near that of graphite. Copper was selected principally to serve as a standard for comparison.

a. Apparatus

A schematic diagram of the experimental arrangement used is shown in Figure 21. The radiation source consisted of a parallel-connected bank of 3 Sylvania Type DFA 150 watt projection lamps. These lamps reach maximum intensity in approximately 80 milliseconds and contain built-in pre-focussed reflectors, so that an object can be heated over a region whose area is proportional to the distance between it and the lamp. The lamps were arranged to produce a nearly homogeneous intensity over an area having a 3/4-inch diameter. Homogeneity was evidenced by scanning a roughened surface of a massive copper heat sink with an infrared radiometer, on which the lamps were focussed, and observing the diffusely reflected infrared radiation. A heat sink was used so that self-emitted radiation could be neglected during observation.

The infrared detection instrument used was a Barnes Engineering Co. Industrial Infrared Radiometer, Model R4D1. The infrared wavelength band passed by its germanium filter is 1.8 to 25 microns (a peak wavelength of 10 microns for a Planck's black body radiation distribution corresponds to a temperature of approximately 300 degree K). This radiometer has four desirable features for this application: (1) its response time is as fast as 10 milliseconds; (2) it can be easily focussed to a circular field of view having a diameter as small as 1/16 inch at a target-detector distance of 30 inches; (3) its temperature sensitivity was 0.5 degree C in the manner used; and (4) it contains an offset control which can suppress reflected radiation so that small temperature variations riding on top of a large signal can be observed at its voltage output terminals

A Sanborn Model 152-100B two-channel, recorder was used for all measurements. Four principle features of this unit are: (1) a writing response time of approximately 30 milliseconds; (2) a sensitivity of 0.001 volts/mm deflectipn; (3) a chart speed variable up to 100 mm/sec; and (4) it contains a timer-marker.



7603809

Figure 22 SCHEMATIC DIAGRAM OF THE EXPERIMENTAL ARRANGEMENT USED TO MEASURE THERMAL CONDUCTIVITY

A photocell was used to monitor heat pulse initiation by observing the visible radiation reflected from the specimens. Its signal was fed into the second channel of the recorder. Although pulse initiation could be determined from the radiometer's signal when observing the total reflected and self-emitted radiation components on the full scale of the recorder, the photocell's signal was necessary to determine pulse initiation when the reflected component was suppressed with the radiometer's offset control.

b. Specimens

1.) Dimensions

For a pulse duration of two seconds, all materials studied appear semi-infinite for thicknesses greater than 1 inch. This is seen from the values of the critical thicknesses, L_{∞} , listed in Table II. Thus, copper, aluminum, steel and lead were conveniently fabricated into one-inch cubes. Areal dimensions of 1 in. x 1 in. were chosen to essentially fill the 3/4-inch diameter area undergoing heating. Graphite specimens were conveniently fabricated into blocks that were one-inch thick in the oriented direction with the grain, and 3/4-inch thick in the direction against the grain. The third dimension was one inch.

2.) Coatings

All surface of the specimens were coated by spraying with Krylon flat black lacquer. Coating thickness and its uniformity were not controlled, but it was estimated that the average thickness was no greater than 10^{-4} cm. This surface preparation was necessary to: (1) provide equal and uniform emissivities; and (2) increase emissivity to increase incident radiation absorption and radiation self emission. It is recognized that this lacquer coating causes resistance to heat flow, but it was found to exhibit the highest emissivity for incident radiation of the several coatings examined. Chief among these was Aquadag, which is a colloidal suspension of graphite particles. This substance as a coating exhibits less resistance to heat flow than does the lacquer, but its emissivity is also less. Its chief disadvantage is that it was found to be difficult to apply uniformly and with good adhesion.

c. Procedure

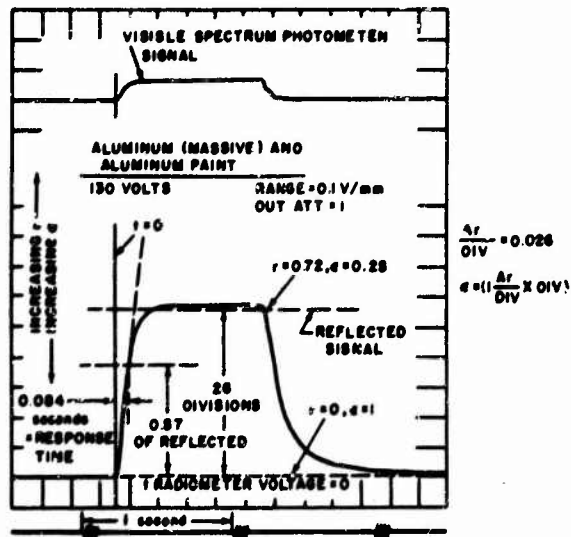
1.) Boundary Conditions

All specimens were mounted snugly into a jig fixture which contained low conductivity rigid plastic walls. The front and rear surfaces, of the specimens, with respect to the incident radiation, were exposed. This fixture served to inhibit lateral heat flow loss as required by the boundary conditions of the technique. Heat loss from the rear surface is actually desirable, since it appears to extend the semi-infinity of the specimens for good conductors. The three projection lamps were focussed onto the front surface over a 3/4-inch diameter area. For the conductivity determinations, the radiometer was focussed into a 1/16-inch diameter area at the center of the heating area. This diameter ratio of 12 was considered sufficient to meet the requirement of plane wave flow through the thickness of the specimen during the observation time.

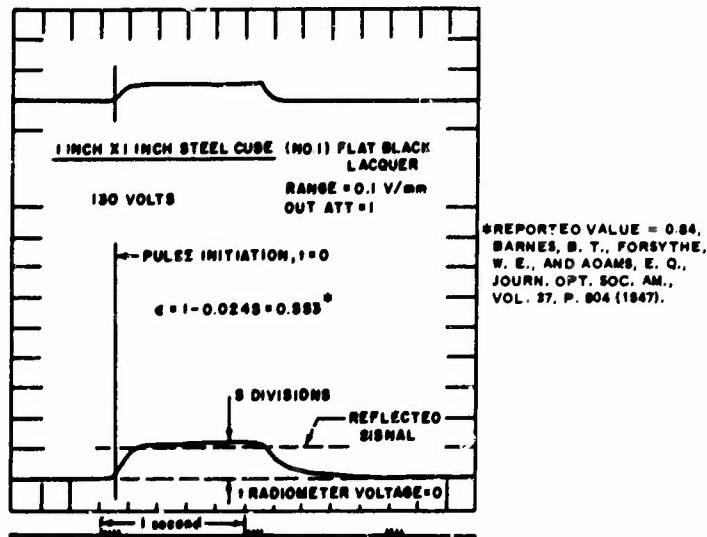
To insure that the specimens appeared semi-infinite during the observation time, the front surface was irradiated while the exposed rear surface was simultaneously monitored with the radiometer. The time delay between pulse initiation and detection serves as a measure of the materials diffusivity, and hence critical thickness ^(25, 26). None of the specimens showed a rear surface temperature rise greater than 0.5 degree C during a pulse duration-observation time of 2 seconds. Thus, all specimens were assumed to be semi-infinite.

2.) Emissivity Measurements

Measurements were performed on all specimens to determine their emissivities. This was accomplished by pulsing the front surface of a coated specimen and simultaneously observing with the radiometer both the reflected and self-emitted infrared radiation components. Since the self-emitted component was small compared to the reflected component the resulting pulse shape appeared almost square with slightly canted skirts. Comparison of the pulse amplitudes of the black lacquer coated specimens with an aluminum painted, massive aluminum heat sink of known infrared emissivity ($\epsilon_\lambda = 0.28$) indicated that the flat black lacquer coating has an $\epsilon_\lambda = 0.85$, which compares favorably with a reported value of 0.84 ⁽²⁷⁾. The actual recordings for the aluminum standard and a coated steel specimen, from which the emissivities have been determined, are shown in Figure 22. Included in this figure are descriptions of the pulse shape characteristics and the geometrical constructions employed.



(a) ALUMINUM PAINTED, MASSIVE ALUMINUM HEAT SINK STANDARD



(b) FLAT BLACK LACQUER COATED STEEL SPECIMEN

760381D

Figure 23 RECORDINGS OF REFLECTED AND SELF-EMITTED RADIATION COMPONENTS FROM WHICH EMISSIVITIES ARE DETERMINED

3.) Conductivity Measurements

For these measurements, the radiometer's offset control was used to suppress almost all of the reflected component of the radiation. The radiometer sensitivity could then be increased to record full scale the voltage (temperature) history of the self-emitted component. Pulse duration and observation were made for 3 seconds rather than for 2 seconds to observe any distortion from the parabolic shape that might result from violation of the condition of semi-infiniteness. Slopes were measured between approximately 1.3 and 2.3 seconds after pulse initiation.

Some typical results of these measurements are shown for graphite specimen No. 34, in Figure 24. In Figure 24 (a) an emissivity recording is shown in which the temperature rise due to self emission can be seen. A temperature scale is also included to illustrate the absolute magnitude of the radiation received by the radiometer. In Figure 24 (b) and (c), the actual recordings of graphite specimen No. 34, against and with the grain direction, are shown, from which thermal conductivities were determined. It is seen that the surface temperature rise for each direction is only a few degrees Centigrade.

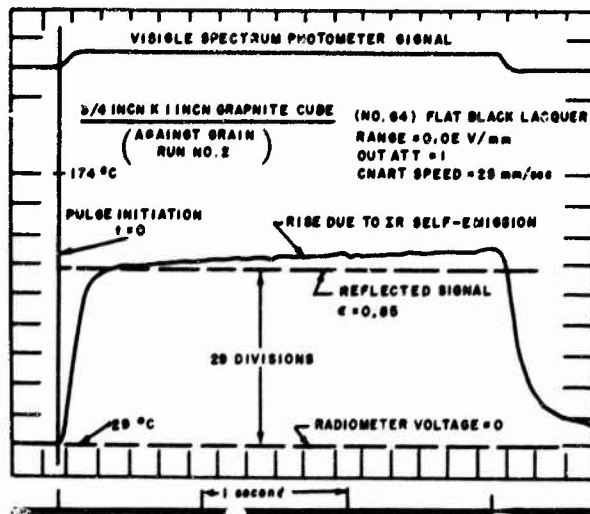
Shown in Figure 25 is a thermal conductivity recording of a large lead fabrication, whose front surface was coated with black lacquer, and which has been pulsed for 6 seconds. Its temperature rise during this period is approximately 9 degrees C.

4. Results and Discussion

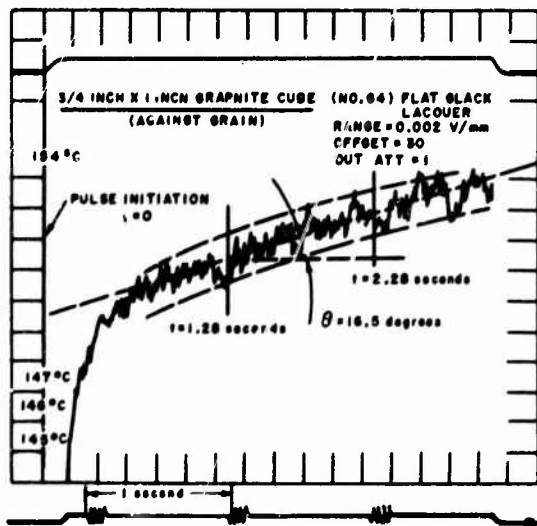
The results of this study are summarized in Tables III and IV. It is seen that the measured infrared emissivities of the flat black lacquer coatings are within approximately 3 percent of 0.88. Differences that occur may be significant, since they are slightly greater than system or measurement errors. As such they are attributed to differences in the base surface finishes.

a. Loss Factors

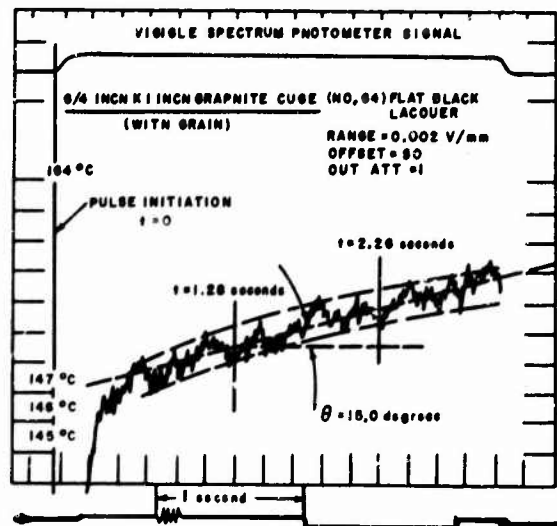
Slopes of the history curves for the specimens are listed in Table III, together with their ratios referenced to the slope for copper. Comparison of these calculated ratios with the experimental results for aluminum, steel and lead indicates that a reasonably constant loss factor, F_1 , of about 2.2 exists. It was not possible to calculate this ratio for the graphite specimens since their densities varied and their conductivities were unknown. This loss factor is believed to arise in part from retardation of the heat flow into the specimens caused by the thermal resistance of the lacquer coating. As indicated in the Theory Section of this report, a consequence of this retardation is to increase the slope of the temperature rise to a degree that is dependent on the heat transfer characteristics of the material. The net effect is to decrease the experimental tangent ratio with respect to its calculated value.



(a) EMISSIVITY MEASUREMENT FOR GRAPHITE SPECIMEN NO. 94
(AGAINST THE GRAIN DIRECTION)



(b) SELF-EMITTED RADIATION HISTORY FROM WHICH THERMAL
CONDUCTIVITY WAS DETERMINED FOR GRAPHITE SPECIMEN
NO. 94 (AGAINST THE GRAIN DIRECTION)



(c) SELF-EMITTED RADIATION HISTORY FROM WHICH THERMAL
CONDUCTIVITY WAS DETERMINED FOR GRAPHITE SPECIMEN
NO. 94 (WITH THE GRAIN DIRECTION)

7408020

Figure 24 EMISSIVITY AND THERMAL CONDUCTIVITY RECORDINGS FOR A
GRAPHITE SPECIMEN

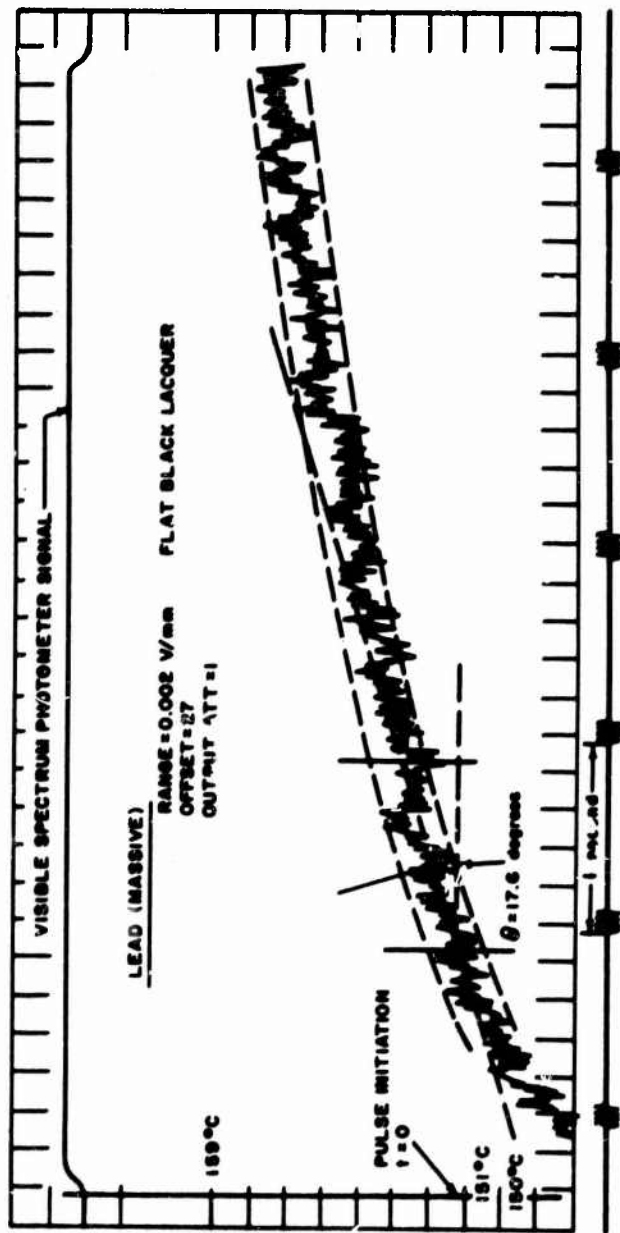


Figure 25 A THERMAL CONDUCTIVITY RECORDING OF A LARGE LEAD FABRICATION,
WHOSE FRONT SURFACE IS COATED WITH FLAT BLACK LACQUER

760383D

Table III: Experimentally measured values of emissivity of lacquer coatings and the measured slopes at the time-temperature histories. Calculated and experimental ratios at $\tan \theta$ and $(k \rho C_p)$ for aluminum, Type 1020 steel, lead and the Type ATJ graphite, referenced to copper.¹

Material	Slope = $\tan \theta$ (measured)	$\left(\frac{cu}{'_{max}}\right)^2 \frac{\tan \theta \text{ material}}{\tan \theta \text{ copper}}$		Tangent Loss Factor	$\frac{(k \rho C_p) \text{ copper}}{(k \rho C_p) \text{ material}}$		Conductivity Loss Factor F_2	Emissivity ϵ_{λ}^{**}
		Calculated	Experimental		Calculated	Experimental		
Aluminum	0.196	1.92	0.90	2.1	2.8	0.85	3.3	0.88
Steel (type 1020)	0.158	3.47	1.5	2.3	8.2	2.4	3.4	0.85
Lead (chem. grade)	0.317	6.20	2.8	2.3	26	7.6	3.4	0.91
Graphite		---	---	---	---	---	---	---
No. 13 (w)	0.268	---	2.5	---	---	6.3	3.3*	0.88
Graphite	0.268	---	2.6	---	---	6.5	---	0.87
No. 13 (Ag)		---	---	---	---	---	---	---
Graphite	0.231	---	2.2	---	---	4.3	---	0.88
No. 16 (w)		---	---	---	---	---	---	---
Graphite	0.212	---	2.1	---	---	4.7	---	0.86
No. 16 (Ag)		---	---	---	---	---	---	---
Graphite	0.249	---	2.4	---	---	5.6	---	0.87
No. 29 (w)		---	---	---	---	---	---	---
Graphite	0.268	---	2.6	---	---	6.8	---	0.86
No. 29 (Ag)		---	---	---	---	---	---	---
Graphite	0.194	---	1.9	---	---	3.5	---	0.88
No. 31 (w)		---	---	---	---	---	---	---
Graphite	0.194	---	1.9	---	---	3.5	---	0.86
No. 31 (Ag)		---	---	---	---	---	---	---
Graphite	0.268	---	2.6	---	---	6.7	---	0.86
No. 34 (w)		---	---	---	---	---	---	---
Graphite	0.296	---	2.8	---	---	8.1	---	0.86
No. 34 (Ag)		---	---	---	---	---	---	---

¹ For copper, $\epsilon_{\lambda} = 0.87$ and $\tan \theta = 0.105$

² Data not available for samples used as indicated by the dash

³ A loss factor of 3.3 was assumed for all graphite specimens in the calculations

⁴ The emissivity measured corresponded to the 1.8 to 25 micron wavelength band observed by the infrared radiometer's germanium-coated, bolometer detector.

TABLE IV. Densities and experimental ratios and values of k for Type ATJ graphite samples for heat flow with and against the direction of the grain orientation.

Graphite Sample Number*	Density ρ (gm/cu cm)	$\frac{k_w}{k_{Ag}}^{**}$	$k_{Ag}^{\dagger} (\frac{\text{cal}}{\text{cm-sec}^{\circ}\text{C}})$	$k_w^{\dagger} (\frac{\text{cal}}{\text{cm-sec}^{\circ}\text{C}})$
13	1.700	1.02	0.13	0.13
16	1.781	1.11	0.17	0.19
29	1.649	1.19	0.13	0.16
31	1.819	1.06	0.23	0.24
34	1.600	1.19	0.11	0.13

*The dimensions of all graphite samples were 3/4" x 1" x 1". The 3/4" x 1" face was perpendicular to the heat flow direction with the grain.

**For highly oriented type ATJ graphite the quantity k_w/k_{Ag} is calculated to equal 1.33 from published data.

†A loss factor of 3.3 was used to obtain these k's for graphite.

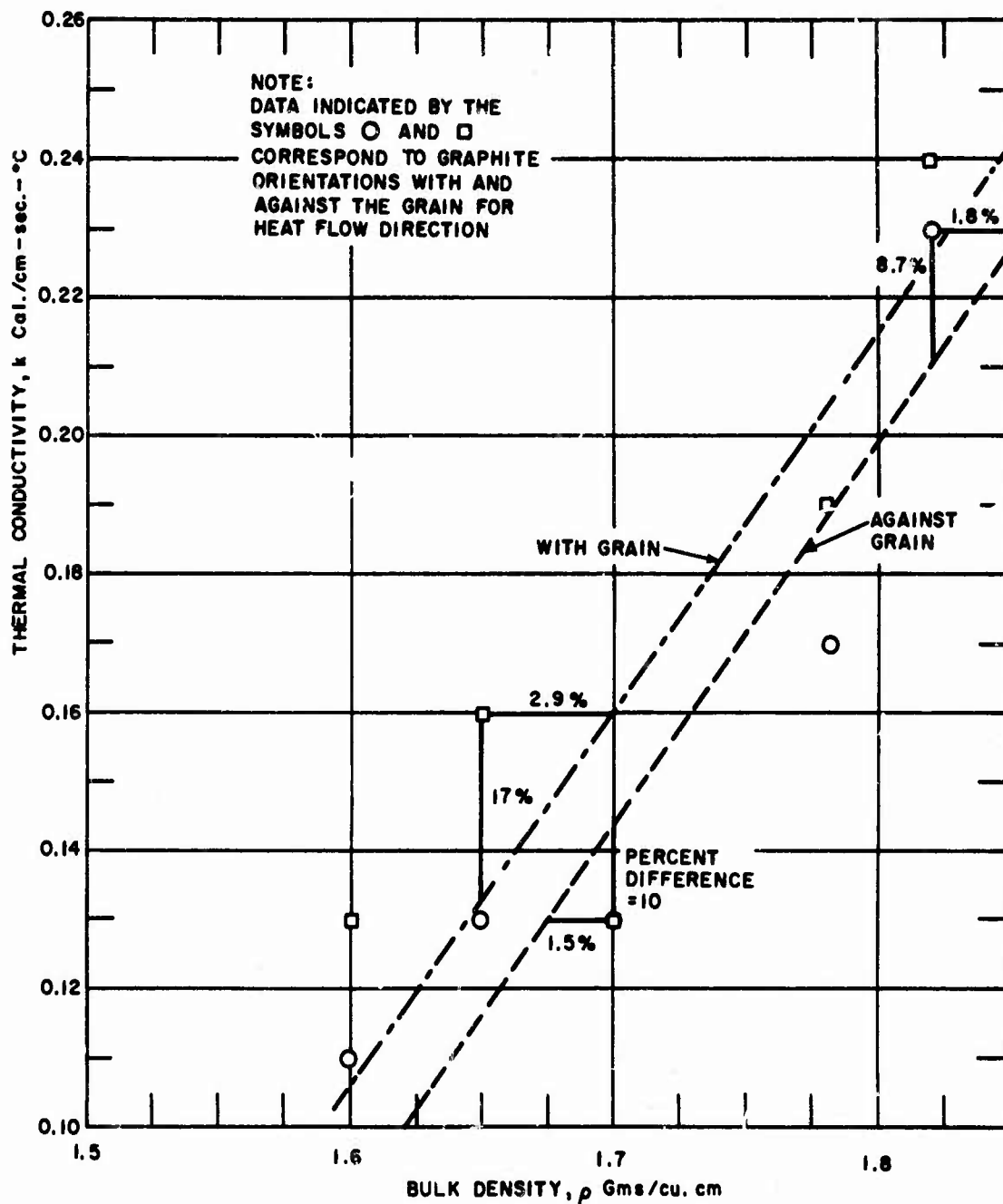
Another contributing effect to F_1 is attributed to lateral heat flow loss which results in nonplanar wave pulse transmission through the specimen. Lateral flow makes a specimen appear to be a better conductor than it really is. This loss is more pronounced in a poorer conductor so that its net effect is to reduce the experimental tangent ratio also, thus increasing the loss factor, F_1 , further. The fact, however, that F_1 appears nearly constant, which indicates a constant shift in experimental values from their calculated values does provide a means for easily adjusting this difference.

The $(k \rho C_p)$ ratios referenced to copper, from which the conductivities are determined, are also included in Table III, together with their corresponding calculated-to-experimental loss factors, F_2 . These factors are seen to center about a value of 3.3, and are similar in their origins as for F_1 .

b. Graphite Conductivities

Listed in Table IV are the densities and the experimentally determined, grain-oriented conductivity ratios for the 5 graphite specimens studied. It is seen that the conductivities in a direction with the grain are consistently greater than the conductivities against the grain, regardless of density. These ratios are to be compared to a value of 1.33 calculated from published data for highly oriented, Type ATJ graphite having a density of 1.7 gms/cm^3 . In partial explanation of this difference, it is to be noted that the experimental technique necessarily results in values, which are representative of only a localized region, whereas the densities of the specimens are bulk values.

Also included in Table IV are the conductivities of the graphite specimens in directions with and against the grain. These values were determined using a loss factor, F_2 , equal to 3.3 and referenced to copper. These experimental conductivities are to be compared to published values of 0.28 and 0.21 cal/cm-sec-degC, with and against the grain, respectively. The experimental values are seen to be generally lower than the reported values, which suggests that either F_2 is less than 3.3 for graphites, or the specimens have lower conductivities in actuality than the reported values. Unfortunately, steady-state conductivity measurements were not performed on any of the specimens due to their geometry. However, had these measurements been performed, they would have validity only for the bulk specimens. The experimental conductivities of the specimens as a function of their densities are plotted in Figure 26. It is seen that conductivity is proportional to density, as expected, such that a one percent change in density produces approximately a 6 percent change in conductivity.



760354D

Figure 26 THERMAL CONDUCTIVITY OF GRAPHITE SPECIMENS VERSUS DENSITY

c. Error Analysis

Contributions to the errors involved in determining the thermal conductivities arise from: (1) instrumentation; (2) geometrical construction on the history curves; and (3) differences between published, or "standards", values and experimental values. Errors in the precision of the instrumentation are estimated to be within 2 percent. Since a comparative technique was used, knowledge of the errors in the accuracy of the instrumentation is unnecessary.

The probable error in determining thermal conductivity is estimated to be 17 percent. This estimate was arrived at by determining the error from each contributing factor in Equation (32) and then calculating the probable error by taking 0.67 of the square root of the sum of the squares of each error contribution. The emissivity error was estimated as 2 percent and the maximum slope error as 21 percent. The slope error arises from the uncertainty in constructing the mean of a history curve when system noise is significant. This uncertainty can be diminished greatly if: (a) a longer observation time is used to increase the abscissa of the slope (which requires using larger specimens); and/or (b) a more intense heat source is used to increase the slope of the temperature rise and suppress noise by reducing radiometer sensitivity. If, for example, a construction time of 2 seconds had been used instead of the 1 second selected in this study, the probable error in determining conductivity would have been approximately 9 percent rather than 17 percent.

The scatter in the conductivity vs. density data, plotted in Figure 26, is attributed mainly to the construction error. An additional source of contribution to the scatter is attributed to local density variations existing within a specimen, having a measured bulk density, which influences the history curve during the observation period.

V.

CONCLUSIONS AND RECOMMENDATIONS

Highlights of the capability developed during this contract are summarized below. It is to be noted that many of these conclusions were identified during the first year's work, and have been extended to other grades of interest to the Air Force during the second year.

1) The predominant material variable influencing the properties of interest in bulk graphite for ablative applications has been identified and experimentally verified to be bulk density. Total volume porosity, which can be calculated from bulk density measurements via graphite's theoretical density, of discrete volumes has been noted as an important parameter in studies of erosion rate in rocket nozzle inserts.

2) A state-of-the-art nondestructive radiation gauging technique, which was developed during the first year, has been extended to all grades of interest, and can be used to determine density in discrete volumes of billets and hardware of these grades to within $\pm 1\%$. As mentioned above, this capability leads to the determination of total volume porosity within the same discrete volumes where radiation measurements are taken.

3) Nondestructive ultrasonic longitudinal-wave velocity measurements have been correlated to elastic modulus, both with and against the grain, for the grades investigated. Combined use of velocity measurements and radiometrically determined density have been correlated uniquely to elastic modulus to provide determination of this property to within 0.06×10^6 psi and, by virtue of a tensile test parameter identified herein as the secant modulus, such measurements can also be used to determine ultimate tensile strength to within ± 300 psi. It is particularly significant to note that tripling the range of values of these mechanical properties correlations to include new grades studied within the past year does not alter the correlations significantly.

4) Based upon the thermoelastic experimentation and analysis made during this contract, as well as the related studies of wave propagation in anisotropic elastic media, it seems plausible that a qualitative NDT parameter for comparing the relative resistance of graphite materials to thermal shock can be obtained empirically. Verification, of course, will require extended study.

5) Based on limited experimentation reported herein, the determination of the thermal conductivity of small graphite fabrications near room temperature is feasible using a nondestructive, one surface, transient heating, comparative technique. It is estimated that the accuracy of this infrared technique is presently within 17% of the standard used for comparison. Extension of this technique to include large fabrications is also feasible. Furthermore, it is believed that the technique can be applied to solids, in general, at elevated temperatures. Validation of the technique, however, will require extended study.

6) Using this technique it was noted that a one percent change in the density of ATJ graphite corresponds to as much as a 6 percent change in its thermal conductivity, illustrating the influence of density on a thermal property, and the sensitivity of this technique to variations of this magnitude. Limitations in the accuracy for nondestructive infrared measurement of conductivity are those associated with the mechanics of geometrical construction used in the technique.

7) Practical aspects of the accomplishments noted above are that, within the limits of the NDT/properties correlations described, determination of density/porosity and mechanical properties can be made by use of these state-of-the-art techniques in discrete volumes on billets and, with minor technique adjustments for changes in geometry, on finished hardware components, thereby providing an assessment of these properties for increased reliability, which would otherwise not be possible. The feasibility of a practical, one-sided, infrared technique for measuring thermal conductivity has also been demonstrated.

The following recommendations are offered on the basis of progress made to date and described in this report, and the knowledge obtained through these studies as to specific areas where consideration should be given to extended and additional studies.

1) It is recommended that the correlation program and NDT technique development be continued on graphite covering the individual and combined application of radiometric, ultrasonic, and infrared tests to obtain correlations of a unique nature with properties and behavior characteristics of interest for ablative applications.

2) It is recommended that better insight into thermal shock phenomena, as well as failure mechanisms in general, can be achieved by:

- a. experimental investigation of wave phenomena at elevated temperatures
- b. triaxial tests over a range of temperatures and orientations
- c. routine tension, compression and torsion tests at orientation intermediate to "against" and "with the grain" directions
- d. multiaxial stress experiments

3) It is recommended that infrared technique development and related studies be extended to determine limitations that may exist, and to improve on these where possible. as well as to adapt these techniques to practical field use. Specifically, work is necessary to:

- a. determine the effect of coatings and their thickness on retardation of heat flow into the solid
- b. establish the uniformity of heat flux and the ratio of diameters of the heating area and radiometer field of view necessary to achieve a desired degree of reliability and accuracy in fabrications having various configurations
- c. determine the radiation source strength and type most suitable for various applications
- d. determine minimum instrumentation requirements
- e. explore methods to facilitate data readout and analysis

4) It is recommended that action be taken to promote, demonstrate and field test the applicable NDT for benefit of producers, fabricators, and users of graphite materials. Such activity will assist in the development and qualification inspection of improved graphite grades, and better identify the failure modes and mechanisms which frustrate the development of design models for ablative applications.

Appendix I.

Wave Propagation in Transversely Isotropic Media

a. Wave Propagation

The stress-strain laws of plane isotropy can be written as

$$\begin{aligned} \epsilon_1 &= \frac{\sigma_1}{E_1} - \frac{\nu_{21}}{E_1} (\sigma_2 + \sigma_3) \\ \epsilon_2 &= -\frac{\nu_{21}}{E_1} \sigma_1 + \frac{\sigma_2}{E_2} - \frac{\nu_2 \sigma_3}{E_2} \\ \epsilon_3 &= -\frac{\nu_{21} \sigma_1}{E_1} - \frac{\nu_2 \sigma_2}{E_2} + \frac{\sigma_3}{E_2} \\ \gamma_{12} &= \frac{r_{12}}{G_{12}} = \gamma_{13} = \gamma_{23} = 2 \frac{(1 + \nu_2)}{E_2} r_{23} \end{aligned} \quad (1)$$

These stress-strain laws can be used with the strain displacement and the equilibrium equations:

$$\begin{aligned} \epsilon_{ij} &= \frac{1}{2} \left(\frac{\partial U_i}{\partial X_j} + \frac{\partial U_j}{\partial X_i} \right) \\ \frac{\partial \sigma_1}{\partial X_1} + \frac{\partial r_{12}}{\partial X_2} + \frac{\partial r_{13}}{\partial X_3} &= \rho \frac{\partial^2 U_1}{\partial t^2} \end{aligned} \quad (2)$$

$$\frac{\partial r_{12}}{\partial X_1} + \frac{\partial r_2}{\partial X_2} + \frac{\partial r_{23}}{\partial X_3} = \rho \frac{\partial^2 U_2}{\partial t^2}$$

$$\frac{\partial r_{13}}{\partial X_1} + \frac{\partial r_{23}}{\partial X_2} + \frac{\partial \sigma_3}{\partial X_3} = \rho \frac{\partial^2 U_3}{\partial t^2}$$

$$\begin{aligned} A \frac{\partial^2 U_1}{\partial X_1^2} + \frac{G_{12}}{2} \left(\frac{\partial^2 U_1}{\partial X_2^2} + \frac{\partial^2 U_1}{\partial X_3^2} \right) + \left(B + \frac{G_{12}}{2} \right) \left(\frac{\partial^2 U_2}{\partial X_1 \partial X_2} + \frac{\partial^2 U_3}{\partial X_1 \partial X_3} \right) \\ = \rho \frac{\partial^2 U_1}{\partial t^2} \end{aligned} \quad (3)$$

$$\begin{aligned} C \frac{\partial^2 U_2}{\partial X_2^2} + \frac{G_{12}}{2} \left(\frac{\partial^2 U_2}{\partial X_1^2} + \frac{\partial^2 U_2}{\partial X_3^2} \right) + \left(B + \frac{G_{12}}{2} \right) \frac{\partial^2 U_1}{\partial X_1 \partial X_2} \\ + \left(D + \frac{G_{12}}{2} \right) \frac{\partial^2 U_3}{\partial X_2 \partial X_3} = \rho \frac{\partial^2 U_2}{\partial t^2} \end{aligned} \quad (4)$$

Appendix I (Cont'd)

$$C \frac{\partial^2 U_3}{\partial X_3^2} + \frac{G_{12}}{2} \left(\frac{\partial^2 U_3}{\partial X_1^2} + \frac{\partial^2 U_3}{\partial X_2^2} \right) + \left(B + \frac{G_{12}}{2} \right) \frac{\partial^2 U_1}{\partial X_1 \partial X_3} + \left(D + \frac{G_{12}}{2} \right) \frac{\partial^2 U_2}{\partial X_2 \partial X_3} = \rho \frac{\partial^2 U_3}{\partial t^2} \quad (5)$$

where

$$A = \frac{E_1 (1 - \nu_2^2)}{\left(1 - \nu_2^2 - 2 \nu_2 \nu_{21}^2 \frac{E_2}{E_1} - 2 \nu_{21}^2 \frac{E_2}{E_1} \right)} \quad (6)$$

$$B = \frac{E_2 (\nu_{21} + \nu_2 \nu_{21})}{\left(1 - \nu_2^2 - 2 \nu_2 \nu_{21}^2 \frac{E_2}{E_1} - 2 \nu_{21}^2 \frac{E_2}{E_1} \right)} \quad (7)$$

$$C = \frac{E_2 - \nu_{21}^2 \frac{E_2^2}{E_1}}{\left(1 - \nu_2^2 - 2 \nu_2 \nu_{21}^2 \frac{E_2}{E_1} - 2 \nu_{21}^2 \frac{E_2}{E_1} \right)} \quad (8)$$

$$D = \frac{\nu_2 E_2 + \nu_{21}^2 \frac{E_2^2}{E_1}}{\left(1 - \nu_2^2 - 2 \nu_2 \nu_{21}^2 \frac{E_2}{E_1} - 2 \nu_{21}^2 \frac{E_2}{E_1} \right)} \quad (9)$$

Kolsky⁽⁸⁾, as well as many others, has presented the correct wave equations for anisotropic elastic media. For the sake of completeness of discussion, they are listed here. As an example of solutions of the equations of motion, consider the case of plane waves in an infinite transversely isotropic medium. Take a wave with its normal in the direction of the axis, X_1 .

$$U_j = A_j \cos \xi X_1 \exp^{i\omega t} \quad j = 1, 2, 3 \quad (10)$$

These may now be substituted into the displacement equation of motion. The corresponding secular equation can then be derived. After applying the necessary condition for non-trivial solution, i. e., setting the determinant of the equation equal to zero:

$$\left(\rho \omega^2 - B \xi^2 \right) \left(\rho \omega^2 - \frac{G_{12}}{2} \xi^2 \right) \left(\rho \omega^2 - \frac{G_{12}}{2} \xi^2 \right) \quad (11)$$

with the resulting wave velocities

$$\sqrt{\frac{G_{12}}{\rho}} \quad (12)$$

Appendix I (Cont'd)

$$\sqrt{\frac{E_2}{\rho} \left(\frac{\nu_{21} + \nu_2 \nu_{21}}{1 - \nu_2^2 - 2 \nu_2 \nu_{21}^2 \frac{E_2}{E_1} - 2 \nu_{21}^2 \frac{E_2}{E_1}} \right)} \quad (13)$$

For graphite, because of the small Poisson's ratio ($\nu_{21} \approx .06$, $\nu_2 \approx .10$) for room temperature, the wave velocity can be very closely approximated by $\sqrt{E_2/\rho}$.

However, for elevated temperatures, these Poisson's ratios increase to .26 and .40. In addition to the marked thermal effects, apparent directionally dependent strain rate influences have been reported⁽⁹⁾, for the Poisson's ratio.

b. Coupled Thermoelastic Stress Wave Phenomena

Existing thermal stress analysis for anisotropic elastic media is based on linear, uncoupled, quasi-static thermoelastically and therefore the solutions are satisfactory for equilibrium conditions^(28, 29). Weng, for example, has considered the problem of thermal stresses in anisotropic hollow cylinders and has shown some of the effects of anisotropy. He reports thermal shock parameters of the form

$$T_B \sigma_{\theta}^* = \bar{\sigma}_{\theta} \left[\frac{E_z - \nu_{zr}^2 E_r}{E_r E_z (a_z \nu_{zr} + a_r)} \right] \quad (14)$$

$$T_B \sigma_z^* = \bar{\sigma}_z \left[\frac{E_z - \nu_{zr}^2 E_r}{E_z (\nu_{rz} a_r E_r + a_z \bar{E}_z)} \right] \quad (15)$$

However, in the strictest sense, no reasonable mathematical solutions have been obtained for the thermal shock problem involving the determination of the transient temperature and stress distribution.

By appealing to the appropriate stress-strain laws, the equilibrium equations, conservation of mass and energy and the laws of thermodynamics, the coupled anisotropic thermoelastic field equations can be formulated. In particular, the partial differential equation governing the temperature field is

$$\begin{aligned} K_1 \frac{\partial^2 T}{\partial X_1^2} + K_2 \frac{\partial^2 T}{\partial X_2^2} + K_3 \frac{\partial^2 T}{\partial X_3^2} = \rho C_v \frac{\partial T}{\partial t} \\ + \frac{T_0}{\beta} \left[\frac{a_1}{E_2^2} (1 - \nu_2^2) + \frac{2a_2}{E_1 E_2} (\nu_{21} + \nu_2 \nu_{21}) \right] \frac{\partial \epsilon_1}{\partial t} \\ + \frac{T_0}{\beta} \left[\frac{a_2}{E_1 E_2} (1 + \nu_2) + \frac{a_1}{E_1 E_2} (\nu_{21} + \nu_2 \nu_{21}) \right] \frac{\partial \epsilon_2}{\partial t} \\ + \frac{T_0}{\beta} \left[\frac{a_2}{E_1 E_2} (1 + \nu_2) + \frac{a_1}{E_1 E_2} (\nu_2 \nu_{21} + \nu_{21}) \right] \frac{\partial \epsilon_3}{\partial t} \end{aligned} \quad (16)$$

Appendix I (Cont'd)

where

$$\beta = \frac{(1 - 2\nu_2 \nu_{21}^2 - 2\nu_{21}^2)}{E_1^2 E_2} - \frac{\nu_2^2}{E_1 E_2^2}$$

$K_i, i = 1, 2$ are thermal conductivities

$\alpha_1, \alpha_2 =$ thermal expansion coefficients

The equation is unmanageable but serves to illustrate the complexities introduced by the more realistic field equations.

It is interesting to compare equation (16) to the corrected "heat" equation of isotropic thermoelastic media^(30, 31).

$$K \left(\frac{\partial^2 T}{\partial X_1^2} + \frac{\partial^2 T}{\partial X_2^2} + \frac{\partial^2 T}{\partial X_3^2} \right) - \rho C_v \frac{\partial T}{\partial t} + (3\lambda + 2\mu) \alpha T_0 \left(\frac{\partial \epsilon_1}{\partial t} + \frac{\partial \epsilon_2}{\partial t} + \frac{\partial \epsilon_3}{\partial t} \right) \quad (17)$$

The directionally dependent materials properties of (16) are seen to modify the transient thermal response. Engineering calculation of thermal stresses are ordinarily carried out in two steps:

1) an estimate of the temperature distribution is obtained from Fourier's heat conduction equation

$$K \left(\frac{\partial^2 T}{\partial X_1^2} + \frac{\partial^2 T}{\partial X_2^2} + \frac{\partial^2 T}{\partial X_3^2} \right) = \rho C_v \frac{\partial T}{\partial t} \quad (18)$$

2) next, the stresses are calculated from the equations of elasto-statics.

Comparing this procedure to the solution of the more exact equation (17), one can see that two effects are omitted: the effect on temperature distribution of straining the body and the dynamic effect due to inertia forces.

Appendix II: Mechanical Properties Data*

Billet No.	Specimen No.	Direction	Bulk Density grams/cc	Dynamic Modulus E _d · 10 ⁶ psi	Tensile Modulus E _t · 10 ⁶ psi	Ultimate Tensile Strength, psi	Total Strain to Failure (in/in)
ATJ 1	1-1	Against Grain	1.726	1.02	1.02	2180	0.0037
	1-2	"	1.718	1.02	0.85	2550	0.0047
	1-3	"	1.714	1.03	0.85	2460	0.0046
	1-4	"	1.725	1.05	0.84	1200	(flaw) - 0.0018
	1-5	"	1.761	1.14	1.00	3010	0.0050
	1-6	With the Grain	1.798	1.81	1.82	4230	0.0038
	1-7	"	1.749	1.67	1.52	3830	0.0038
	1-8	"	1.729	1.57	1.47	2890	0.0029
	1-9	"	1.722	1.53	1.67	3570	0.0036
	2-1	Against Grain	1.683	1.02	0.83	2360	0.0043
	2-2	"	1.686	1.00	0.79	2630	0.0048
	2-3	"	1.689	1.01	0.78	2480	0.0045
	2-4	"	1.706	1.02	0.85	2480	0.0045
	2-5	"	1.750	1.09	1.01	2580	0.0042
	2-6	With the Grain	1.721	1.51	1.39	3350	0.0036
	2-7	"	1.729	1.54	1.43	3450	0.0035
2-8	"	1.743	1.54	1.52	3360	0.0035	
2-9	"	1.683	1.30	1.54	2480	0.0029	
2-10	Against Grain	1.746	1.09	0.88	2440	0.0042	
2-11	With the Grain	1.672	1.22	1.14	2550	0.0034	
2-12	Against Grain	1.754	1.08	0.86	2780	0.0052	
2-13	With the Grain	1.696	1.34	1.22	2370	0.0028	
ATJ 2	A-1	Against Grain	1.693	0.99	0.99	2330	0.0040
	A-2	"	1.697	.98	0.99	2430	0.0043
	A-3	"	1.706	.99	0.91	2170	0.0036
	A-4	"	1.713	1.02	0.92	2750	0.0047
	A-5	"	1.693	1.05	1.00	2770	0.0044
	A-6	"	1.699	1.05	0.92	2850	0.0047

Appendix II: Mechanical Properties Data*(Continued)

Billet No.	Specimen No.	Direction	Bulk Density grams/cc	Dynamic Modulus E _d · 10 ⁶ psi	Tensile Modulus E _t · 10 ⁶ psi	Ultimate Tensile Strength, psi	Total Strain to Failure (in/in)
ATJ 2	A-7	Against Grain	1.701	0.99	0.93	2470	0.0039
	A-8	"	1.708	1.01	0.90	2700	0.0046
	W-1	With the Grain	1.737	1.71	1.57	4120	0.0038
	W-2	"	1.710	1.59	1.52	3820	0.0037
	W-3	"	1.693	1.56	1.50	3020	0.0028
	W-4	"	1.707	1.53	1.45	3310	0.0033
	W-5	"	1.665	1.45	1.40	2350	0.0022
	W-6	"	1.673	1.47	1.47	3480	0.0036
ATJ 3	W-7	"	1.693	1.49	1.48	3470	0.0036
	W-8	"	1.728	1.60	1.54	3560	0.0032
	X-1	Against Grain	1.764	1.17	0.97	2790	0.0040
	X-2	"	1.743	1.16	0.78	3070	0.0048
	X-3	"	1.742	1.15	0.84	2920	0.0044
	X-4	"	1.759	1.18	0.86	3370	0.0055
	X-5	"	1.760	1.18	1.27	2860	0.0040
	Y-1	With the Grain	1.760	1.65	1.31	4260	0.0042
RVA 1	Y-2	"	1.747	1.58	1.56	4020	0.0038
	Y-3	"	1.745	1.58	1.25	3240	0.0031
	Z-1	"	1.755	1.63	1.46	4070	0.0039
	Z-2	"	1.758	1.62	1.55	4370	0.0042
	Z-3	"	1.754	1.64	1.40	4170	0.0039
	Y-1	Against Grain	1.853	1.19	0.96	1420	0.0020
	Y-2	"	1.849	1.23	1.06	1560	0.0020
	Y-3	"	1.854	1.23	0.92	1770	0.0025
	Y-4	"	1.835	1.28	0.97	1900	0.0024
	Y-5	"	1.836	1.27	1.01	2030	0.0028
	X-1	With the Grain	1.833	1.44	1.17	2020	0.0023
	X-2	"	1.840	1.45	1.01	2030	0.0023
	X-3	"	1.841	1.46	1.20	2260	0.0026
	X-4	"	1.860	1.53	1.33	2640	0.0026
	X-5	"	1.859	1.56	1.27	2750	0.0029

Appendix II: Mechanical Properties Data* (Continued)

Billet No.	Specimen No.	Direction	Bulk Density grams/cc	Dynamic Modulus E _d , 10 ⁶ psi	Tensile Modulus E _t , 10 ⁶ psi	Ultimate Tensile Strength, psi	Total Strain to Failure (in/in)	
RVA 1	Z-1	With the Grain	1.848	1.49	1.22	2400	0.0027	
	Z-2	"	1.847	1.49	1.29	2220	0.0024	
	Z-3	"	1.860	1.54	1.10	2280	0.0023	
	Z-4	"	1.851	1.55	1.33	2680	0.0028	
	Z-5	"	1.850	1.56	1.23	2390	0.0025	
RVA 2	RA1	Against Grain	1.820	1.35	← Broken in machining →			
	RA2	"	1.808	1.28	1.08	2110	0.0031	
	RA3	"	1.828	1.32	0.97	2360	0.0035	
	RA4	"	1.817	1.27	0.79	2050	0.0033	
	RA5	"	1.818	1.27	0.75	1990	0.0033	
	RA6	"	1.823	1.36	1.15	2440	0.0036	
	RA7	"	1.817	1.31	0.95	2390	0.0039	
	W-1	With the Grain	1.831	1.65	1.45	2950	0.0031	
	W-2	"	1.828	1.64	1.33	2990	0.0031	
	W-3	"	1.824	1.69	1.31	3050	0.0033	
	CFW 1	A-1	Against Grain	1.813	1.28	← Selected for compression tests →		
		A-2	"	1.809	1.20	1.06	1910	0.0028
		A-3	"	1.813	1.21	1.02	2100	0.0032
A-4		"	1.796	1.16	← Selected for compression tests →			
A-5		"	1.798	1.18	1.08	2220	0.0036	
A-6		"	1.801	1.19	0.97	2080	0.0034	
W-1		With the Grain	1.811	1.64	← Selected for compression tests →			
W-2		"	1.813	1.71	← Selected for compression tests →			
W-3		"	1.805	1.72	1.17	2620	0.0027	
W-4		"	1.816	1.73	1.36	2790	0.0027	
W-5		"	1.819	1.67	1.21	2780	0.0029	
W-6	"	1.820	1.61	1.52	2870	0.0029		
W-7	"	1.800	1.69	1.35	2970	0.0030		
W-8	"	1.788	1.63	1.46	2760	0.0028		
W-9	"	1.802	1.73	1.52	2930	0.0028		
W-10	"	1.796	1.63	1.21	2560	0.0027		
W-11	"	1.799	1.69	1.28	2790	0.0029		

Appendix II: Mechanical Properties Data* (Continued)

Billet No.	Specimen No.	Direction	Bulk Density grams/cc	Dynamic Modulus E_d , 10 ⁶ psi	Tensile Modulus E_t , 10 ⁶ psi	Ultimate Tensile Strength, psi	Total Strain to Failure (in./in.)
CFW 1	W-12	With the Grain	1.797	1.66	1.38	2810	0.0029
	A-7	Against Grain	1.802	1.24	1.08	2100	0.0030
CFW 2	A-8	"	1.806	1.32	1.25	2330	0.0031
	A-9	"	1.817	1.29	0.95	2330	0.0036
	A-10	"	1.820	1.26	0.96	2170	0.0034
	A-11	"	1.818	1.27	1.23	2060	0.0028
	A-12	"	1.837	1.28	1.04	2220	0.0032
	W-13	With the Grain	1.819	1.70	1.47	2760	0.0026
	W-14	"	1.812	1.66	1.59	2850	0.0029
	W-15	"	1.812	1.625	1.32	2800	0.0030
	W-16	"	1.812	1.64	1.42	2850	0.0030
	W-17	"	1.799	1.645	1.50	2720	0.0029
	W-18	"	1.809	1.70	1.55	2940	0.0028
	W-19	"	1.802	1.63	1.50	3030	0.0032
	W-20	"	1.806	1.67	1.45	2840	0.0027
W-21	"	1.817	1.75	1.72	2950	0.0027	
W-22	"	1.820	1.69	1.59	3110	0.0032	
W-23	"	1.818	1.70	1.45	2960	0.0029	
W-24	"	1.837	1.72	1.47	3260	0.0030	
ZTA 1	1-A	Against Grain	1.916	0.92	0.71	1330	0.0029
	2-A	"	1.918	0.91	0.82	1710	0.0039
	3-A	"	1.926	0.93	0.82	1630	0.0034
	4-A	"	1.931	0.89	0.75	1690	0.0038
	1-C	"	1.907	0.77	0.84	1530	0.0036
	2-C	"	1.900	0.89	0.84	1570	0.0037
	3-C	"	1.894	0.94	0.87	1660	0.0039
	4-C	"	1.890	0.90	0.79	1460	0.0030
	5-C	"	1.893	0.90	0.83	1470	0.0032
	6-C	"	1.895	0.89	0.85	1680	0.0041
	7-C	"	1.909	0.91	0.83	1780	0.0045

Appendix II: Mechanical Properties Data * (Continued)

Billet No.	Specimen No.	Direction	Bulk Density grams/cc	Dynamic Modulus E _d , 10 ⁶ psi	Tensile Modulus E _t , 10 ⁶ psi	Ultimate Tensile Strength, psi	Total Strain to Failure (in/in)
RVA (-1)	D1	Against Grain	1.873	2.23	1.72	2300	0.0018
	D2	"	1.863	1.76	1.69	2130	0.0017
	D3	"	1.875	1.83			
	D4	"	1.883	1.85			
	B1	With the Grain	1.872	2.60	2.38	2840	0.0015
	B2	"	1.885	2.71	2.74	3370	0.0017
CFZ1	B3	"	1.873	2.64			
	1	Against Grain	1.877	1.21			
	2	"	1.889	1.25			
	3	With the Grain	1.893	2.00	1.85	3280	0.0026
	4	"	1.875	1.78	1.67	2930	0.0025
	5	"	1.876	1.73			
	6	"	1.874	1.80			

*Object in selecting specimens from each billet was to obtain the maximum range in these properties as indicated by the NDT response rather than to obtain a statistical average of random samples.

APPENDIX III.

Test Methods for Determination of Physical Properties of Graphite

1. **Bulk Density:** Bulk density was determined by dividing the mass of a specimen by its bulk volume. The conventional unit is grams/cc.
2. **Specific Resistance:** Specific resistance was determined by measuring the potential drop along the length of a specimen of known geometry with a given current flow. Measurements were made at room temperature.
3. **Dynamic Modulus:** Room temperature modulus measurements were performed by the resonant frequency vibration technique with the specimen supported at two points as a beam.
 - a. **Equipment:** Type FM-500 Elastomat, Magnaflux Corp.
 - b. **Specimen Geometry:** 1 1/8" diameter by 6" nominal length
4. **Tensile Properties**
 - a. **Equipment:** Instron Model TTC tensile testing machine
 - b. **Strain Rate:** Constant to failure 0.005 in/in/min.
 - c. **Temperature:** 75° F ± 2° F
 - d. **Tensile Specimen:** Over-all length of 5 inches, gauge diameter 0.400 inches.
 - e. **Strain:** Measured by ASTM Class B 1 extensometers having a 2-inch gauge length

REFERENCES

1. G. E. Lockyer, Investigation of Nondestructive Methods for the Evaluation of Graphite Materials, AFML-TR-65-113 (1965).
2. C. E. Waylett, M. B. Carter, M. A. Spring, Research and Development on Advanced Graphite Materials, WADD TR 61-72, Volume XXXI - Impregnation of Graphite.
3. M. F. Berard, L. Swope, Evaluation of the Firing Behavior of Selected Grades of Graphite, Authors report No. MF-532, IDEP No. 501.00.00.00-Q3-01.
4. R. B. Dull, Research and Development on Advanced Graphite Materials, WADD TR 61-72, Volume XXVI - Physical Properties of Some Newly Developed Graphite Grades.
5. "The Industrial Graphite Engineering Handbook," Union Carbide Corporation, Carbon Products Division.
6. Nightingale, R. E., Nuclear Graphite, Academic Press, 1962.
7. Signorelli, R. A., J. R. Johnston, "Erosion Resistance and Failure Mechanisms of Several Nozzle Materials in a Small Solid - Propellant Rocket Engine," NASA TND-1658, February 1963.
8. Kolsky, "Stress Waves in Solids".
9. F. J. Digesu and C. D. Pears, "The Determination of Design Criteria for Grade CFZ Graphite," AFML-TR-65-142, May 1965.
10. F. J. Digesu, C. D. Pears, "The Lateral Strain Behavior of Graphite - An Anisotropic Material," A paper presented at the Seventh Biennial Conference on Carbon, Cleveland, Ohio, 1965.
11. R. Hill, "A Theory of Strength for the Yielding and Plastic Flow of Anisotropic Metals," Proc. of Royal Society, Series A, Vol. 193, pp. 281-297, 1948.
12. V. D. Azzi and S. W. Tsai, "Anisotropic Strength of Composites," Presented at Spring Meeting of the Society for Experimental Stress Analysis, " May 1965 and published in Experimental Mechanics.
13. S. W. Tsai, "Strength Characteristics of Composite Materials," NASA CR-224, April 1965.
14. E. M. Leno, "Deformation and Failure of Granular Media under Three Dimensional Stresses," Experimental Mechanics, February 1966.

15. A. M. Freudenthal, H. Geringer, "Mathematics of the Inelastic Continuum," *Handbuch der Physik*, Springer Verlag, 1958, pg. 427-428.
16. V. V. Sokolovsky, "Statics of Earthly Media," *I. Z. Datersvo Akademii Noah S. SR Moscow*, 1942.
17. W. J. Parker, R. J. Jenkins, C. P. Butler, G. L. Abbott, "Flash Method of Determining Thermal Diffusivity, Heat Capacity and Thermal Conductivity," *J. Appl. Phys.* 32, 1679 (1961).
18. R. L. Rudkin, R. J. Jenkins, and W. J. Parker, "Thermal Diffusivity Measurements on Metals at High Temperatures," *Rev. Sci. Instr.*, 33, 21(1962).
19. H. W. Deem, and W. D. Wood, "Flash Thermal-Diffusivity Measurements Using a Laser," *Rev. Sci. Instr.*, 33, 1079 (1962).
20. J. V. Beck and H. Hurwicz, "Study of Thermal Discontinuities and Associated Temperature Disturbances in a Solid Subject to a Surface Heat Flux, Part II," *Avco Technical Report, TR-9-59-14*, April 28, 1959, p. 9.
21. H. S. Carslaw and J. C. Jaeger, "Conduction of Heat in Solids," Oxford, London, 2nd ed. (1959), p. 75.
22. *The Industrial Graphite Engineering Handbook*, Union Carbide Corp., (1964), p. 5B.05.01.
23. Carslaw, *op. cit.*, pp. 20, 73.
24. *Ibid.* p. 76.
25. R. E. Taylor and J. A. Cape, "Finite Pulse-Time Effects in the Flash Diffusivity Technique," *Appl. Phys. Letters*, Vol. 5, No. 10, November 1964, pp. 212-3.
26. A. W. Schultz, "Final Summary - Infrared NDT Development Studies," *Avco Technical Release, R270-10-66-184*, February 1, 1966, Appendix E.
27. B. T. Barnes, W. E. Forsythe, and E. Q. Adams, *J. Opt. Soc. Am.*, Vol. 37 (1947), p. 804.
28. Lekhnitskii, S., "Theory of Elasticity of An Anisotropic Elastic Body," Holden-Day Inc., San Francisco, 1963.

29. Tu-Lung Weng, "Thermal Stress in Anisotropic Hollow Cylinders," *Journal of Basic Engineering*, June 1965, pg. 391-397.
30. B. A. Boley and I. S. Tolins, "Transient Coupled Thermoelastic Boundary Value Problems in the Half Space," *Journal of Applied Mechanics*, 1962, Vol. 29, Series E, No. 4.
31. B. A. Boley and J. H. Weiner, "Theory of Thermal Stresses," John Wiley and Sons, Inc., New York, 1960.

UNCLASSIFIED

Security Classification

DOCUMENT CONTROL DATA - R&D		
<small>(Security classification of title, body of abstract and indexing annotation must be entered when the overall report is classified)</small>		
1. ORIGINATING ACTIVITY (Corporate author) Avco Corporation Space Systems Division Lowell, Massachusetts		2a. REPORT SECURITY CLASSIFICATION Unclassified
		2b. GROUP
3. REPORT TITLE Investigation of Nondestructive Methods for the Evaluation of Graphite Materials		
4. DESCRIPTIVE NOTES (Type of report and inclusion dates) Summary Report - 15 April 1965 to 14 April 1966		
5. AUTHOR(S) (Last name, first name, initial) Lockyer, G. B., Leno, E. M., and Schultz, A. W.		
6. REPORT DATE July 1966	7a. TOTAL NO. OF PAGES 90	7b. NO. OF REFS 31
8a. CONTRACT OR GRANT NO. AF 33(615)-1601	8b. ORIGINATOR'S REPORT NUMBER(S) AFML-TR-66-101	
a. PROJECT NO. 7360	9a. OTHER REPORT NO(S) (Any other numbers that may be assigned this report) AVSSD-0061-66-RR	
c. TASK NO. 736002		
10. AVAILABILITY/LIMITATION NOTICES This document is subject to special export controls and each transmittal to foreign governments or foreign nationals may be made only with prior approval of the Metals and Ceramics Division (MAM), Air Force Materials Laboratory, Wright-Patterson AFB, Ohio 45433.		
11. SUPPLEMENTARY NOTES	12. SPONSORING MILITARY ACTIVITY Metals and Ceramics Division Air Force Materials Laboratory Wright-Patterson AFB, Ohio 45433	
13. ABSTRACT <p>A program of investigation was begun in April 1964, to determine nondestructive testing methods and techniques for the evaluation and characterization of graphite materials under contract No. AF 33(615)-1601. During the first year, April 1964 to April 1965, the properties and behavior characteristics which are necessary for characterizing graphite as an ablative material for aerospace applications were identified, and applicable NDT methods and techniques were described and theoretically justified. Moreover, the philosophy of Avco's step-wise approach to nondestructive materials evaluation was identified in relation to graphite, and an over-all program plan was established. Correlations between NDT measurements and properties of interest were developed and reported for certain grades of graphite. During the second year, April 1965 to April 1966, these correlations were extended to other grades and, additionally, have been studied in combination in an effort to obtain qualitative response to behavior characteristics such as erosion rate and thermal shock resistance.</p> <p>To this end, nondestructive test methods for evaluating the performance of graphite under complex thermal and mechanical loading conditions were investigated. The observed response of a molded graphite is compared to theoretical predictions, which are based on the constitutive equations for a transversely isotropic media. Also discussed are the limitations of the</p>		

(Continued)

DD FORM 1473
1 JAN 64

UNCLASSIFIED

Security Classification

UNCLASSIFIED
Security Classification

16 KEY WORDS	LINK A		LINK B		LINK C	
	ROLE	WT	ROLE	WT	ROLE	WT
Graphite, Nondestructive Testing (ultrasonic wave velocity, radiometry, infrared), Properties (density, dynamic modulus, tensile modulus, secant modulus, ultimate tensile strength, strain to failure, thermal conductivity, thermal shock, oxidation erosion).						

INSTRUCTIONS

1. **ORIGINATING ACTIVITY:** Enter the name and address of the contractor, subcontractor, grantee, Department of Defense activity or other organization (corporate author) issuing the report.
- 2a. **REPORT SECURITY CLASSIFICATION:** Enter the overall security classification of the report. Indicate whether "Restricted Data" is included. Marking is to be in accordance with appropriate security regulations.
- 2b. **GROUP:** Automatic downgrading is specified in DoD Directive 5200.10 and Armed Forces Industrial Manual. Enter the group number. Also, when applicable, show that optional markings have been used for Group 3 and Group 4 as authorized.
3. **REPORT TITLE:** Enter the complete report title in all capital letters. Titles in all cases should be unclassified. If a meaningful title cannot be selected without classification, show title classification in all capitals in parenthesis immediately following the title.
4. **DESCRIPTIVE NOTES:** If appropriate, enter the type of report, e.g., interim, progress, summary, annual, or final. Give the inclusive dates when a specific reporting period is covered.
5. **AUTHOR(S):** Enter the name(s) of author(s) as shown on or in the report. Enter last name, first name, middle initial. If military, show rank and branch of service. The name of the principal author is an absolute minimum requirement.
6. **REPORT DATE:** Enter the date of the report as day, month, year, or month, year. If more than one date appears on the report, use date of publication.
- 7a. **TOTAL NUMBER OF PAGES:** The total page count should follow normal pagination procedure, i.e., enter the number of pages containing information.
- 7b. **NUMBER OF REFERENCES:** Enter the total number of references cited in the report.
- 8a. **CONTRACT OR GRANT NUMBER:** If appropriate, enter the applicable number of the contract or grant under which the report was written.
- 8b, c, & 8d. **PROJECT NUMBER:** Enter the appropriate military department identification, such as project number, subproject number, system numbers, task number, etc.
- 9a. **ORIGINATOR'S REPORT NUMBER(S):** Enter the official report number by which the document will be identified and controlled by the originating activity. This number must be unique to this report.
- 9b. **OTHER REPORT NUMBER(S):** If the report has been assigned any other report numbers (either by the originator or by the sponsor), also enter this number(s).
10. **AVAILABILITY/LIMITATION NOTICES:** Enter any limitations on further dissemination of the report, other than those

imposed by security classification, using standard statements such as:

- (1) "Qualified requesters may obtain copies of this report from DDC."
- (2) "Foreign announcement and dissemination of this report by DDC is not authorized."
- (3) "U. S. Government agencies may obtain copies of this report directly from DDC. Other qualified DDC users shall request through _____."
- (4) "U. S. military agencies may obtain copies of this report directly from DDC. Other qualified users shall request through _____."
- (5) "All distribution of this report is controlled. Qualified DDC users shall request through _____."

If the report has been furnished to the Office of Technical Services, Department of Commerce, for sale to the public, indicate this fact and enter the price, if known.

11. **SUPPLEMENTARY NOTES:** Use for additional explanatory notes.
12. **SPONSORING MILITARY ACTIVITY:** Enter the name of the departmental project office or laboratory sponsoring (paying for) the research and development. Include address.
13. **ABSTRACT:** Enter an abstract giving a brief and factual summary of the document indicative of the report, even though it may also appear elsewhere in the body of the technical report. If additional space is required, a continuation sheet shall be attached.
It is highly desirable that the abstract of classified reports be unclassified. Each paragraph of the abstract shall end with an indication of the military security classification of the information in the paragraph, represented as (TS), (S), (C), or (U).
There is no limitation on the length of the abstract. However, the suggested length is from 150 to 225 words.
14. **KEY WORDS:** Key words are technically meaningful terms or short phrases that characterize a report and may be used as index entries for cataloging the report. Key words must be selected so that no security classification is required. Identifiers, such as equipment model designation, trade name, military project code name, geographic location, may be used as key words but will be followed by an indication of technical content. The assignment of links, rules, and weights is optional.

UNCLASSIFIED
Security Classification